NASA Contractor Report 198321

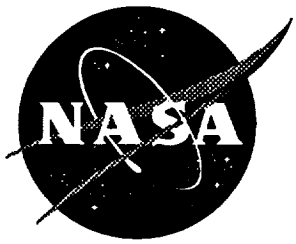

Wind-Tunnel Parametric Investigation of Forebody Devices for Correcting Low Reynolds Number Aerodynamic Characteristics at Spinning Attitudes

C. Michael Fremaux
Lockheed Engineering & Sciences Company, Hampton, Virginia

Contract NAS1-19000

March 1996

National Aeronautics and
Space Administration
Langley Research Center
Hampton, Virginia 23681-0001

Abstract

An investigation has been conducted in the NASA Langley 20-Foot Vertical Spin Tunnel to determine the static aerodynamic characteristics of a 1/25-scale model of the X-29A Forward Swept Wing airplane. The tests were conducted at a free-stream dynamic pressure of 3.6 lb/ft^2, corresponding to a unit Reynolds number of 0.35×10^6/ft, or 0.45×10^5 based on a maximum fuselage forebody depth of 0.128 ft. The purpose of this investigation was to assess the ability of various forebody devices to correct the aerodynamic parameters that are important in spin testing for Reynolds number effects. Low Reynolds number aerodynamic characteristics obtained for the X-29A during the present test were compared with high Reynolds number data obtained for this configuration in a previous test. The low Reynolds number tests were conducted first with the unmodified (baseline) model and then repeated with each of several forebody modifications installed.

Introduction

Reynolds number effects are well known to be a potential source of discrepancy between measured aerodynamic characteristics from sub-scale model tests and actual flight results. Free-spin tests of dynamically scaled models (as well as rotary balance tests) are performed at Reynolds numbers on the order of 1.0×10^5 at the NASA Langley Research Center. In terms of predicting the spin behavior of modern, fuselage-loaded (i.e., negative values of the inertia yawing moment parameter, IYMP) fighter designs from low-Reynolds-number free spin or rotary balance data, the crossflow over forebodies with certain cross-sectional shapes has been shown to be the major source of these Reynolds number effects if they exist (refs. 1-6). Historically, the majority of spin modes predicted using the free spin and rotary balance techniques have correlated well with full-scale results (where comparable full-scale results were available). But forebody-dominated effects have been found to be so severe for certain geometries as to make the model spin and spin-recovery characteristics unrepresentative of those for the airplane (e.g. the F-5A, ref. 5). However, modifications were identified for the F-5A and other model configurations that resulted in the successful prediction of full-scale spin modes from free spin tests.

There are no high-Reynolds number free-spin wind tunnels in existence, and few high Reynolds-number facilities equipped with rotary balances (e.g., see refs. 7 and 8). Consequently, the method that has most often been used to analyze a model's susceptibility to Reynolds number effects has been to compare static force and moment data obtained at spinning attitudes (high angles of attack and sideslip) and low Reynolds numbers to that acquired at relatively high Reynolds numbers. When a discrepancy is noted between the low- and high-Reynolds-number data trends, forebody modifications are commonly used in an attempt to correct for these effects.

This does not imply that static data can be used to accurately predict the forces and moments on a configuration during a spin. It has been demonstrated over many years of research and testing that modeling rotational effects (as on a rotary balance) is essential to properly measure spin aerodynamics. For example, static yawing moment coefficient values at a given angle of attack may be antispin over the entire sideslip range tested, but a fast, flat spin could still exist at that angle of attack.

The primary assumption made in the present research (as well as that of refs. 5, 6, and 9) is as follows: if the static aerodynamic trends of the parameters most important in a spin are reasonably corrected for Reynolds number effects (most significantly, there are no sign differences between low- and high-Reynolds number data), then the rotary aerodynamic trends will be similarly corrected. This presumes that the static data have been obtained using a test technique that approximates the flow over the component known to be sensitive to Reynolds number (the forebody in the present case) during a spin. It should be noted that the tests of ref. 9 using a model of the Northrop T-38 airplane (a 2-seat trainer of which the F-5 series are derivatives) included rotary balance tests at various Reynolds numbers. However, the Reynolds number range for these tests was small, and static tests similar to those in refs. 5 and 6 over a wider range of Reynolds numbers were

also used. Further explanation of the rational for using static data in this manner is found in the *Results and Discussion* section below.

Strakes mounted on the fuselage nose or forebody have been most often used to correct for Reynolds number effects (refs. 3, 5, 6, and 9), although forebodies with highly-modified cross-sectional shapes have also been tried (ref. 6). The grit-type boundary layer transition strips discussed in references 10 and 11 have not typically been used for this application. Factors such as very low Reynolds number coupled with the large and variable angles of attack and sideslip would tend to make the required grit size quite large compared to that used in standard wind tunnel tests.

Of the aerodynamic characteristics typically most affected by forebody-dominated Reynolds number effects at spinning attitudes (yawing moment, pitching moment, side force, and normal force), yawing moment is the most important of these parameters in the dynamics of a spin. The yawing moment is especially important in the high-angle-of-attack (flat) spin that is characteristic of many modern fighters. The use of forebody strakes has been reasonably successful at correcting static yawing moment trends, at least at high angles of attack (α>70° for the F-5A in ref. 5 and α>80° for the X-29A in ref. 6). However, some strake geometries can adversely affect pitching moment (i.e., reduce the static longitudinal stability of the basic model) beyond the reduction in longitudinal stability typically associated with low Reynolds number testing at high angles of attack. While a small-to-moderate increment in positive (nose-up) pitching moment would probably not affect the spin characteristics of a model with a high degree of static longitudinal stability, more modern configurations with relaxed longitudinal stability could be affected due to a large proportion of the available nose-down pitching moment being offset.

As noted above, a given forebody modification may not provide the desired static aerodynamic characteristics over the entire α- and β-range tested. In practice, an iterative procedure might therefore be required in to determine whether or not a "fix" is possible. The static characteristics would be used to determine the attitudes at which Reynolds number effects are prevalent. The unmodified baseline model would then be free-spin tested to identify the uncorrected spin mode(s). If a baseline spin mode were to occur at an attitude for which Reynolds number effects are probable, then forebody modifications could (hopefully) be tailored to work at that attitude. Free-spin tests would then be repeated with the modifications installed.

The goal of the present test was to identify non-actuated forebody devices that met or exceeded the ability of traditional strakes to correct yawing moment for Reynolds number effects while not having their adverse effect on pitching moment. These results were intended to be used for identifying forebody devices that provided the best overall performance (relative to each other), even at test attitudes that might not correlate with the uncorrected predicted spin modes of the "testbed" X-29A model (i.e., the spin modes predicted by the iterative procedure described above). The devices were required to be simple to fabricate and install while being rugged enough to survive the rigors of free-spin testing with dynamically-scaled models. The X-29A was chosen for this test because it represents a contemporary design with relaxed static longitudinal stability and has a forebody known to be sensitive to Reynolds number effects. In addition, high Reynolds number data were available for comparison from the previously-cited reference 6.

A caveat is in order concerning the results of this study. The use of forebody devices for modifying aerodynamic characteristics is known to be extremely configuration dependent. While it is assumed (as stated above) that the findings reported here will be useful in a general sense as a guide and starting point for using forebody devices on other configurations, direct application of the results apply strictly to the X-29A, or other fighter airplanes equipped with the F-5A forebody. In other words, the final suitability any device for correcting Reynolds number effects should be verified experimentally for each model configuration under consideration.

Symbols

b	wing span, ft
C_m	pitching moment coefficient, $\frac{M_Y}{q_\infty S\bar{c}}$
C_n	yawing moment coefficient, $\frac{M_Z}{q_\infty Sb}$
C_{n_β}	directional stability derivative, $\frac{\partial C_n}{\partial \beta}$
C_Y	side force coefficient, $\frac{F_Y}{q_\infty S}$
$\bar{c}$	wing mean aerodynamic chord, ft
F_Y	side force, lb
h	height of "triangular patch" boundary layer stimulator, in
M_Y	pitching moment, ft-lb
M_Z	yawing moment, ft-lb
M_∞	free stream Mach number
q_∞	free stream dynamic pressure, lb/ft^2
Re	Reynolds number based on some characteristic length
Re_c	critical Reynolds number for boundary layer transition
S	wing area, ft^2
V_∞	free stream velocity, ft/sec
α	angle of attack, deg
β	sideslip angle, deg
β_{eff}	effective sideslip angle on forebody due to rotation about spin axis, deg
ΔC_m	pitching moment increment
δ_a	flaperon deflection, deg
δ_c	canard deflection, deg
δ_r	rudder deflection, deg
δ_s	strake flap deflection, deg
Ω	spin rate about vertical axis, rad/sec
$\frac{\Omega b}{2V}$	nondimensional spin rate, positive for erect spin to pilot's right

Abbreviations:

BL	airplane buttline, in
c.g.	center of gravity
FS	airplane fuselage station, in
IYMP	inertia yawing moment parameter, $\frac{I_X - I_Y}{mb^2}$
WL	airplane waterline, in

Model

An existing 1/25-scale free-spin model of the X-29A Forward Swept Wing airplane was modified at the NASA Langley Research Center and tested statically on the rotary balance apparatus in the Langley 20-Foot Vertical Spin Tunnel. The dimensional characteristics of the full-scale airplane are presented in table 1. A three-view drawing of the X-29A model is shown in figure 1. The model/sting/rotary balance arrangement is illustrated in figure 2. A photograph of the baseline model appears in figure 3.

For all tests, the control surfaces were fixed at "high-α" deflections (δ_c = -60°, δ_a = 25°, δ_s = 30°, and δ_r = 0°) that are representative of those typically used in free-spin testing. The flaperon/wing geometry of the current model deviated from the full-scale arrangement (as well as that of the model in ref. 6) in that the model flaperons extend out to the wing tip, whereas the airplane flaperons do not. In addition, neither flap actuator fairings on the wing nor flow-through engine inlets were represented on the model. These difference in geometry were not expected to significantly affect the comparison of results from the present test with those of previous tests.

Test Facility and Conditions

The low Reynolds number, static force and moment tests were performed in the Langley 20-Foot Vertical Spin Tunnel, which is described

in reference 1. The tests were performed in the Spin Tunnel so that the flow environment would be similar for the present static tests and any future free-spin tests. The investigation was performed at a free stream dynamic pressure (q_∞) of 3.6 lb/ft^2, which corresponds to a unit Reynolds number (Re) of 0.35×10^6/ft (0.45×10^5 based on a maximum fuselage forebody depth of 0.128 ft) and a Mach number (M_∞) of 0.05. The model was sting-mounted on the Spin Tunnel's rotary balance arm, which was not rotated for the present tests.

An internally-mounted, six component strain gage balance attached to an aft-entry sting was used to measure forces and moments, which were resolved into the appropriate coefficients about a body axis system (fig. 4). The moment reference center was at FS 454.27 ($-0.05\bar{c}$), WL 66, and BL 0 (full scale), while the balance reference center was at FS 582.63, WL 75.3, and BL 0 (also full scale). The small internal volume of the model near the moment reference center necessitated locating the balance a greater distance from the moment reference center than is customary. The angle of attack range used in these tests was α=40° to α=90° while the sideslip angle was varied from β=-15° to β=+30°. The model was not tested in an inverted attitude.

Wind tunnel boundary corrections were not applied to the data due to the small size of the model as compared to the test section (the model wing span was 5.5% of nominal test section diameter) and because drag data were not required. No attempt was made to correct for flow angularity. Aside from the forebody devices mentioned previously, boundary layer transition strips were not used for this test.

Add-On Forebody Devices

In this section, a description of each forebody device tested is presented, along with a brief summary of the reasoning used in choosing each device. In all cases (with the exception of the helical trip wire), the devices were installed in the same location on the model's forebody as that used in references 2 and 3, i.e., no attempt was made to optimize the location of the strakes. Details of the forebody devices and their installation locations are shown in figures 5 through 7.

Four of the five forebody devices used in this study can generally be classified into one (or both) of two categories: those that produce strong, 2-dimensional vortices that emanate from a definite separation line at their edges (such as side-mounted strakes) and 3-dimensional devices that energize the boundary layer, causing transition and (presumably) delaying separation. Devices of the first type do not correct for Reynolds number effects in the sense that the flow about the forebody is necessarily forced to be more reflective of the high-Re case. Rather, they can be tailored to favorably influence certain aerodynamic forces and moments (such as C_Y and C_n) acting on the model, by reducing vortex asymmetries on the forebody, for example. However, there may be a trade-off in the sense that other aerodynamic parameters could be adversely affected (e.g., C_m). In contrast, devices of the second type could potentially produce low-Re flow about the forebody that more closely resembles the flow at high Re (if they were efficient at tripping the boundary layer and were properly located), thus beneficially influencing both the yawing moment and pitching moment coefficients. Assuming that both types of devices performed adequately, the ultimate effect would be the same in that there would be less discrepancy between the measured aerodynamic parameters at low and high Reynolds numbers.

Typical nose strakes (e.g., strake 1 discussed below) fall into the first category. Strakes 3 and 4 belong to the second category. Strake 2 is a hybrid that has characteristics of both categories. Helical trips have traits in common with nose strakes in that they also force boundary-layer separation, but in a manner that suppresses, rather than causes, vortex formation. Further discussion of the mechanisms involved in the workings of each of the forebody devices are discussed briefly below.

Strake 1

Strake 1 (figs. 5a and 6a) is a solid, 2-dimensional forebody strake that was developed for the F-5A free-spin model to correct for Reynolds number effects (ref. 5).

Likewise, this same strake geometry was used during wind-tunnel Reynolds number tests of the X-29A (referred to as a "lateral strake" in ref. 6) since the F-5A and X-29A have a similar forebody shape (The X-29A airplane forebody is eleven inches shorter than that of the F-5A and is equipped with small nose strakes - see ref. 12). In both cases, strake 1 was found to adequately correct the yawing moment characteristics of the configurations so as to give reasonable free-spin test results. However, this strake had the unwanted side effect of adding a sizable positive (nose-up) pitching moment increment to both the F-5A and X-29A. In the case of the F-5A, the relatively high degree of longitudinal stability of the basic airframe meant that the addition of the strakes reduced, but did not eliminate, its nose-down pitching moment characteristics over the range of angle of attack and sideslip angle tested, even at low Reynolds number. In contrast, the basic X-29A has only marginally longitudinal stability at high angles of attack (e.g., see ref. 6) and the addition of a large nose-up pitching moment increment can cause it to become unstable. In both cases, however, it was determined that strake 1 was the best compromise between correcting yawing moment and adversely affecting pitching moment. Unpublished results for the X-29A, along with the results for the F-5E (a derivative of the F-5A with the same forebody shape - see ref. 13) indicate that the addition of strake 1 to these models was successful in correcting their free-spin characteristics in that the models exhibited flat spin modes characterized by slower spin rates, lower angles of attack, and faster recoveries when equipped with strakes than when the strakes were removed.

Strake 2

Figures 5b and 6a illustrate the geometry and location of strake 2. Essentially, the "outline" dimensions of strake 1 were retained but the planform shape was modified by cutting adjacent 60-degree serrations to form a "sawtooth" pattern. The geometry of strake 2 was based on the results of reference 14. In that work, the performance of solid, nonplanar "Gurney" flaps on a wing (analogous to strake 1) was improved by the incorporation of serrations. In particular, it was concluded that the serrations introduced streamwise vortices into the flow which favorably influenced the separation of the upper-surface boundary layer. For the present study, it was assumed that the serrated strake 2 would also fix the separation line on the forebody (like strake 1) but would be more efficient at energizing the boundary layer. It was also assumed that strake 2 would induce less nose-up pitching moment than strake 1 due to its reduced planform area (i.e., area normal to the flow at high angles of attack).

Strake 3

A very interesting approach to the problem of causing low Reynolds number boundary layers to transition from laminar to turbulent flow is addressed in references 15, 16, and 17. The authors of these reports developed a device which they dubbed the "triangular patch boundary layer stimulator". Essentially, the triangular patch resembles the serrated strake 2, except that the serrations are directed into the flow when the model is at high angles of attack (figs. 5c and 6b). Therefore, "strake" 3 is not shaped like a strake in the traditional sense. As with strake 2, the premise behind this device is that a 3-dimensional shape is more effective at promoting boundary layer transition than one that is 2-dimensional. The convergence region between each triangle of strake 3 causes the local flow to accelerate rapidly, and to then stream off as a small vortex as it leaves the juncture between the triangles. The relatively close spacing of the triangles produces a large number of vortices to stimulate transition.

In reference 17, it was stated that the critical Reynolds number (Re_c) for a triangular patch stimulator attached to a flat plate was approximately 60, which is an order of magnitude lower than Re_c for grit-type trips. Using this number, the thickness of the patches for the present test was initially estimated to be 0.003 inches. This value was arrived at by assuming that the forebody at high angles of attack could be represented as a 2-dimensional circular cylinder and then using the methods of reference 18. However, the value of Re_c= 60 in reference 16 was arrived at by observing the occurrence of transition at some distance well down stream of the device (approximately 5 times the thickness, or "height" (h) of the patch - see fig. 5c) and under idealized conditions on a flat plate. Since the forebody is

neither flat nor likely to operate under ideal conditions in the present study, it was felt that a significantly greater height would be required to force transition to occur immediately behind the strake (the same reasoning for not using standard grit-type trip strips). As a practical consideration, fiberglass sheet material with a thickness of 0.033 inches was available and was used to fabricate strake 3. The strake was attached to the model such that the junctures of the serrations were aligned with the attachment line of strakes 1 and 2 (fig. 6b).

Strake 4

To account for the possibility that the height of strake 3 was still too small to provide the required yawing moment correction in these tests, strake 4 was fabricated by doubling the height of strake 3 (0.066 in.) but otherwise maintaining the same geometry (fig. 5c). The installation point on the model was the same as for strake 3 (fig. 6b).

Helical trip wire

In reference 19, a helical trip wire was developed to alleviate side-force asymmetries on slender, pointed forebodies at high angle of attack. The unusual shape of the helical trip gives it an advantage over the more commonly used straight trip wire in that its curved shape forces separation from the forebody to occur at different peripheral locations, thus causing the flow velocity to vary at the separation point along the length of the trip. Unlike a straight wire or traditional strake, the non-uniform vortex shedding produced by the helical trip wire "(disrupts) the formation of discrete 2-dimensional vortex cores....and thus the possibility of vortex asymmetry is removed at the source" (ref. 19).

In reference 19, the forebodies (either isolated or mounted on generic fuselage/wing combinations) were tested at angles of attack from 0° to 55°, and primarily at zero sideslip (limited tests of the effect of the trips on lateral/directional stability were conducted at β=10°). In reference 20, a complete airplane model (the F-15A) was tested both with standard forebody strakes and the helical trip wire based on the work of reference 19. Angles of attack of up to 55° were also tested, but at greater sideslip angles (β=±20°) than in reference 19. These results showed that the helical trip wire was very effective at eliminating or reducing zero-β asymmetries in yawing moment while being much less prone than strakes to generate large, positive pitching moment increments. In fact, the trip wire typically provided more nose-down pitching moment at a given angle of attack than the forebody without any devices attached, presumably by reducing the high-α crossflow drag on the forebody at the low Reynolds number of the test (0.59×10^6 based on mean aerodynamic chord of the wing). Conflicting results as to the effect of the helical trip wires on directional stability (C_{n_β}) at relatively small sideslip angles were obtained in references 19 and 20, suggesting that their impact on this parameter is configuration dependent (ref. 19). Although there were no data in either reference to support the effectiveness of the helical trip wire at the significantly higher angles of attack (up to 90°) and sideslip (up to 30°) of the present tests, it was felt that the impressive results at lower α and β warranted its inclusion.

In reference 20, it was concluded that the minimum height to ensure good performance of the helical trip could not be precisely calculated. However, a "rule of thumb" for determining a starting point for the wire size was given as "2% of the maximum forebody diameter". Using this guideline, a wire diameter of approximately 0.03 inches was calculated. But it was assumed, as with strakes 3 and 4, that the calculated size would likely be too small for the trip to be effective at the large sideslip angles of the present test. Therefore, standard solder wire (used due to its pliability) with a diameter of 0.06 inches was used to fabricate the helical trip. The general arrangement of the helical trip wire installation on the X-29A model is shown in figure 7.

Results and Discussion

An explanatory figure, along with the results of the X-29A static tests (with and without add-on forebody devices) are presented in figures 8 - 12. Based on the findings of references 5 and 6 concerning the relative

importance of various aerodynamic characteristics on the spin of the F-5A and X-29A, only the yawing moment coefficient and pitching moment coefficient are considered in this report. Figures 9 and 10 illustrate the yawing moment characteristics of the model, while figures 11 and 12 show the pitching moment characteristics. In each figure, low Reynolds number data for the clean model ("baseline") are plotted along with that for the model equipped with each of the 5 forebody devices tested. As a benchmark, high Reynolds number data for a 1/8-scale model of the X-29A without any forebody devices are reproduced from reference 6. These data are labeled in figures 9 - 12 as "Re=5x10^6/ft" for convenience, although the reproduced data from reference 6 were actually obtained at Reynolds numbers ranging from 4.92x10^6/ft to 5.2x10^6/ft (1.97x10^6 to 2.1x10^6, respectively, based on a maximum fuselage forebody depth of 0.4 ft).

Yawing Moment Characteristics

In figure 9, C_n is plotted as a function of β for constant values of α. Note that in certain figures (e.g., fig. 9a) the data in the vicinity of β=0° indicate that the model was directionally stable (i.e., the slope of the C_n-versus-β curve was positive). However, the nonzero-sideslip angles in the present tests were meant to provide a simulation of the flow over the model's forebody during a spin caused by a combination of vertical descent rate and rotation rate. This is termed the forebody's "effective" sideslip angle in references 3 and 4. Therefore, a positive static sideslip represents the conditions that the model's forebody would experience in an erect spin to the pilot's right. Thus, quadrants 1 and 3 of explanatory figure 8 are prospin and quadrants 2 and 4 are antispin. For perfectly steady spins (i.e., non-oscillatory spins such as those simulated on most rotary balances), small sideslip angles are representative of the forebody crossflow low spin rates, while large values of β are used to simulate the effect of high spin rates. However, during free-spin tests in which oscillations about all three axes are typical, the effective sideslip angle (as well as the angle of attack) are also oscillatory. Therefore, care must be taken when interpreting the static data so that potential Reynolds number effects are taken into account in the correct range of attitudes. Unless otherwise noted, the following analysis will concentrate on results at positive sideslip angles (i.e., simulating right spins), but the results should generally be applicable to spins in either direction.

At α=40° (fig. 9a), both the low-and high-Re data had similar positive slopes and magnitudes for sideslip angles between +5 and -5, as stated previously. Between β=0° and β=10°, all of the yawing moment data were primarily prospin. Just beyond β=10°, the high-Re coefficients became negative (antispin), but the low Reynolds number data remained non-negative (prospin). Note that there was a slight decrease in magnitudes of the prospin moments provided by the forebody devices as compared to the baseline case.

Excluding small zero-β offsets, the high-Re data in figures 9b-9i (α=50° to α=90°) indicated that the static yawing moment characteristics of the X-29A were antispin in the α- and β-ranges tested. In contrast, the low-Re baseline data showed significant prospin moments for α=50° through α=85° (figs. 9b-9h). This trend is consistent with the findings of reference 6. The low-Re prospin tendencies of the unmodified X-29A generally lessened as the angle of attack increased. At α=90°, the baseline yawing moment coefficient was antispin over the entire β-range.

Next, the effects of the add-on forebody devices are examined in figure 9. It is immediately evident that strake 3 (the thinner of the two "triangular patches") had little effect on the low-Re results in that data trends with this strake installed closely followed the baseline results at nearly all attitudes. The effect of strake 3 on yawing moment will not be considered further in this report except to point out unusual characteristics in the data. From α=40° to α=65° (figs. 9a - 9d), none of the forebody devices eliminated all of the prospin tendencies. By α=70° (fig. 9e), strake 4 and the helical trip had essentially eliminated the prospin moments, but the data for the other strakes were still prospin in the vicinity of β=5°. At α=75°, strakes 1 and 2 also produced antispin C_n over the entire β-range tested. Strakes 1, 2, and 4 continued to generate antispin yawing moment coefficients at α=80° and α=85°. Note that at α=80°, use of the helical trip resulted in

essentially zero yawing moment for $\beta=\pm5°$, but at $\alpha=85°$, C_n was again clearly antispin. At $\alpha=90°$, all of the low Reynolds number results (including those for the baseline mentioned previously) showed antispin trends.

The angle of attack range in which the forebody devices were effective is better illustrated in figure 10. Note that in figures 10b and 10d, the high-Re results of ref. 6 were obtained at $\beta=-4°$ and $\beta=+4°$, respectively, while those at low Reynolds number were for $\beta=-5°$ and $\beta=+5°$.

At zero sideslip (fig. 10c), there were significant yawing moment offsets in the low-Re data between $\alpha=45°$ and $\alpha=75°$ (and up to $\alpha=85°$ for strake 3). None of the devices tested provided enough of a stabilizing influence on the forebody flow to correct these zero-sideslip offsets to the high-Re values.

The results for non-zero sideslip are studied next. At $\beta=5°$ (fig. 10d), none of the forebody devices provided significant improvement over the baseline case until approximately $\alpha=70°$. At this angle of attack, strake 4 and the helical trip were the most effective. However, the effectiveness of both devices was reduced (i. e., the magnitude of the antispin yawing moment was reduced) as the angle of attack approached $\alpha=80°$, and then increased again between $\alpha=80°$ and $\alpha=90°$ (this reduction in effectiveness was also evident in the negative sideslip data - figs. 10a and 10b). In contrast, strakes 1 and 2 produced the correct sign of C_n beginning at approximately $\alpha=75°$ and got progressively more effective as the angle of attack approached 90°. Possibly, there was a flow mechanism in this α-range associated with the X-29A forebody shape that "overpowered" the smaller devices (strake 4 and the helical trip wire), but did not effect the relatively large strakes 1 and 2. As the sideslip angle was increased between $\beta=5°$ (fig. 10d) and $\beta=30°$ (fig. 10h), the angle of attack at which the low-Re yawing moment coefficients became antispin decreased, including that for the baseline case.

Although the match between the low-Re and high-Re data was improved above $\alpha=70°$, none of the forebody devices produced yawing moment coefficients that closely matched the high-Re data at every sideslip angle. For example, at $\beta=10°$ strake 1 provided a very good match for $\alpha=80°$ and above. At $\beta=15°$, strake 1 still provided the best correction. For $\beta=20°$, the high-Re data were highly nonlinear, and were not matched by any of the forebody device results. By $\beta=30°$, strakes 1 and 2 seemed to overcorrect C_n, while the data for the other forebody devices and the baseline case showed good agreement with the high-Re results for the higher angles of attack.

In summary, none of the forebody devices corrected the low-Re yawing moment coefficients (either in sign or magnitude) over all combinations of α and β tested. Assuming that matching the sign of the high-Re yawing moments is more important than duplicating the magnitudes, then strake 4 and the helical trip (with the exception of a reduction in effectiveness near $\alpha=80°$ for the latter) provide reasonably good performance above approximately $\alpha=70°$ while strakes 1 and 2 provide the correct sign for yawing moment above $\alpha=75°$.

Pitching Moment Characteristics

In references 5 and 6, large destabilizing pitching moment increments due to Reynolds number effects were found for the F-5A and X-29A, respectively. Using the high-Re results of reference 6 for comparison, similar pitching moment increments were evident for the unmodified (baseline) 1/25-scale model of the X-29A in the present tests (figs. 11 and 12).

The basic effect on pitching moment coefficient of adding forebody devices to the model is illustrated in figure 11c. This figure shows the pitching moment coefficient versus angle of attack for the X-29A at zero sideslip. Positive pitching moment coefficient increments (ΔC_m) were found between the high-Re data and low-Re baseline data at all angles of attack. In fact, the sign of C_m was positive between approximately $\alpha=50°$ and $\alpha=80°$ for the low-Re baseline case. In reference 21, low-Re rotary balance pitching moment data were shifted (nose down) by an amount equal in magnitude to the destabilizing increment caused by Reynolds number effects in a static test. Although some of the predicted flat-spin modes were affected only marginally by this C_m shift (up to a 3-degree decrease in angle of attack and a slight

change in the spin rate), in one case an equilibrium spin mode was predicted using the shifted data whereas none had been predicted using uncorrected data. This illustrates that, while yawing moment is of primary importance for flat-spin analysis, large changes in the pitching moment cannot be assumed to be inconsequential. And while it is clear that these large, Reynolds-number-induced pitching moment increments cannot be compensated for by adding forebody devices to the model, it was assumed that one or more of the devices tested would at least not aggravate the problem significantly.

As shown in figure 11c, strake 1 added further sizable destabilizing pitching moment increments (as compared to the low-Re baseline data) over the entire α-range, from a minimum of ΔC_m=+0.1 at α=80° to a maximum of ΔC_m=+0.25 at α=60°. Likewise, strake 2 introduced a large, positive ΔC_m between α=40° and α=75°, but the magnitude of the strake-2 pitching moment increment was always less than that for strake 1. At higher angles of attack, this strake did not significantly affect the pitching moment characteristics of the model, indicating that it might be useful if no low-α spins were indicated by tests of the unmodified spin model.

The boundary-layer-trip devices (strake 3, strake 4, and the helical trip) clearly had less detrimental effect on C_m than strakes 1 and 2. In fact, above α=60° all three devices provided greater nose-down pitching moment than the baseline configuration (with the exception of the helical trip at α=90°). Obviously, the boundary layer trips have smaller projected area normal to the flow over the forebody than do strakes 1 and 2. But the tripping of the boundary layer and subsequent reduction in the crossflow drag on the forebody at high angles of attack was assumed to be the primary reason for the increased nose-down pitching moment as compared to the baseline case. Note that strake 3, although ineffective at correcting the low-Re yawing moment characteristics, caused the pitching moment data to be more nose-down than the baseline case over nearly the entire angle of attack range.

The effect of nonzero sideslip on the pitching moment can be seen in figures 11a and 11b (negative values of β), and 11d through 11h (positive values of β). As with the yawing moment results, the following analysis will concentrate on the positive sideslip angles except as indicated.

Reynolds number effects in the form of large destabilizing pitching moment increments were still evident at all angles of attack for the nonzero sideslip angles. However, both the detrimental effects of strakes 1 and 2, and the beneficial effects of strake 3, strake 4, and the helical trip were generally reduced as the magnitude of β was increased. At β=10° (fig. 11e), all of the low-Re data curves (including that for the baseline) tended to converge between α=80° and α=90°. The angle of attack at which the curves started to converge decreased as β was increased. At β=30° (fig. 11h), there were relatively small differences in the pitching moment coefficients among all of the low-Re curves. The trends noted above are also evident in figure 12, where C_m is plotted as a function of β, with α held constant.

Summary of Results

The results of a static wind-tunnel test to determine the relative effectiveness of several add-on forebody devices at correcting an aerodynamic parameter important to the spin characteristics of the X-29A (yawing moment coefficient) for forebody-dominated Reynolds number effects while minimizing their potential adverse affect on another important parameter (pitching moment coefficient) may be summarized as follows:

1. Significant Reynolds number effects on the pitching moment coefficient of the baseline X-29A were evident at all attitudes tested. These effects were also present in the yawing moment coefficient trends, but were less severe at the highest values of angle of attack and sideslip.

2. The devices were not effective at preventing low-Reynolds-number induced prospin yawing moments over the entire sideslip range tested below α=70°. At α=70° and above, only strake 4 and the helical trip prevented low-Re prospin yawing moments. Both strake 1

and strake 2 eliminated the prospin moments for α=75° and above. Strake 3 was not effective at any angle of attack.

3. While effective at correcting the sign of the low Reynolds number yawing moments above certain angles of attack, none of the devices consistently matched the magnitudes of the high Reynolds number yawing moment data.

4. Strake 1 added a sizable destabilizing pitching moment increment to the zero-sideslip characteristics of the model, in addition to that caused by Reynolds number effects on the baseline configuration. Strake 2 produced a smaller destabilizing increment than did strake 1, and above α=75° this strake had no significant effect on the zero-sideslip pitching moment characteristics of the model.

5. Above α=60°, strake 4 and the helical trip caused the zero-sideslip pitching moment characteristics to be more stable (nose-down) than those for the baseline configuration at low Reynolds number. However, neither of these devices compensated for the large disparity between the baseline low-Re data and the high-Re data.

Concluding Remarks

A static wind tunnel test to measure the forces and moments on a 1/25-scale model of the X-29A Forward Swept Wing airplane has been conducted in the NASA Langley 20-Foot Vertical Spin Tunnel. This research was conducted in order to study a configuration whose aerodynamic characteristics were known to be susceptible to Reynolds number effects on the fuselage forebody at spinning attitudes. Changes in the aerodynamics due to low Reynolds number, especially in the yawing moment, can have a profound effect on the spin modes predicted by either the free-spin or rotary-balance subscale model techniques. Previous tests had predicted that the X-29A free-spin model test results would be pessimistic, (i.e., more prospin) than the airplane spin results.

At present, high Reynolds number aerodynamic data are available primarily from static wind tunnel tests. These data have been used successfully to predict whether or not different airplane designs would be impacted by Reynolds number effects on spin aerodynamics, primarily due to changes in forebody crossflow. When differences due to Reynolds number were noted (especially in the yawing moment), forebody strakes historically were used in an attempt to make corrections, with the assumption that the spin aerodynamics would be similarly corrected. While reasonably good success at correcting the yawing moment has been realized using strakes, there has typically been a penalty in the form of a destabilizing pitching moment increment being added. Less stable pitching moment characteristics may or may not have an effect on the predicted spin modes, primarily depending on the degree of longitudinal stability naturally inherent in a particular configuration. For a contemporary, longitudinally unstable design like the X-29A, the impact could be substantial. The results of this study indicate that other add-on forebody devices (besides traditional strakes) can have beneficial effects on yawing moment that are similar to those produced by strake 1, but with a reduced (strake 2) or even eliminated (strake 4 and the helical trip) destabilizing pitching-moment penalty at certain angles of attack.

The forebody devices in this study (with the exception of strake 1 in ref. 5) were not optimized in terms of size, location, or orientation. Further efforts to optimize three promising shapes (strake 2, strake 4, and the helical trip) should be carried out in future research. In addition, the use of other devices (possibly small aft-mounted strakes) should be studied as a means of compensating for changes in the longitudinal characteristics of free-spin models due to Reynolds number effects.

References

1. Neihouse, A. I.; Klinar, W. J.; and Scher, S. H.: *Status of Spin Research for Recent Airplane Designs.* NASA TR R-57, 1960. (supersedes NACA RM L57F12)

2. Polhamus, E. C.: *A Review of Some Reynolds Number Effects Related to Bodies at High Angle of Attack.* NASA CR 3809, 1984.

3. Chambers, J. R., Anglin, E. L., and Bowman, J. S., Jr.: *Effects of a Pointed Nose on Spin Characteristics of a Fighter Airplane Model Including Correlation with Theoretical Calculations.* NASA TN D-5921, 1970.

4. Chambers, J. R., and Grafton, S. B.: *Aerodynamic Characteristics of Airplanes at High Angles of Attack.* NASA TM 74097, 1977.

5. Kauffman, R. C., Scher, S. H., and Cohen, L. E.: *Static Aerodynamic Characteristics of a 1/7-Scale Model of the F-5A Airplane at Angles of Attack From 0 to 90 Degrees and Angles of Sideslip From -10 to 30 Degrees for a Mach Number of 0.20.* NASA TM X-62,339, 1974.

6. Whipple, R. D. and Ricket, J. L.: *Low-Speed Aerodynamic Characteristics of a 1/8-Scale X-29A Model at High Angles of Attack and Sideslip.* NASA TM 87722, 1986.

7. Tuttle, M. H., Kilgore, R. A., and Sych, K. L.: *Rotary Balances-A Selected, Annotated Bibliography.* NASA TM 4105, 1989.

8. Malcolm, G. N.: "Rotary-Balance Apparatuses". Report of the Fluid Dynamics Panel/Working Group 11, *Rotary-Balance Testing for Aircraft Dynamics-Part 1: Experimental Techniques.* AGARD Advisory Report 265, pp. 22-46, 1990.

9. Bernard, A. V.: *A Qualitative Analysis of the Spin Characteristics of the Northrop T-38 Trainer Airplane.* Northrop Corporation Report-Norair Division, NOR-59-429, 1959.

10. Braslow, A. L. and Knox, E. C.: *Simplified Method for Determination of Critical Height of Distributed Roughness Particles for Boundary Layer Transition at Mach Numbers from 0 to 5.* NACA TN 4363, 1958.

11. Braslow, A. L., Hicks, R. M., and Harris, R. V., Jr.: *Use of Grit-Type Boundary-Layer-Transition Trips on Wind Tunnel Models.* NASA TN D-3579, 1966.

12. Fisher, D. F., Richwine, D. M., and Landers, S.: *Correlation of Forebody Pressures and Aircraft Yawing Moments on the X-29A Aircraft at High Angles of Attack.* NASA TM 4417, 1992.

13. Scher, S. H. and White, W. L.: *Spin-Tunnel Investigation of a 1/20-Scale Model of the Northrop F-5E Airplane (Coord. No. AF-AM-422).* NASA TM SX-3556, 1977.

14. Vijgen, P. M., Van Dam, C. P., Holmes, B. J., and Howard, F. G: "Wind-Tunnel Investigation of Wings with Serrated Sharp Trailing Edges". *Proceedings of the Conference on Low Reynolds Number Aerodynamics,* University of Notre Dame, June 5-7, 1989.

15. Hama, F. R., Long, J. D., and Hegarty, J. C.: "On Transition from Laminar to Turbulent Flow". *Journal of Applied Physics,* Volume 24, pp. 388-394, 1957.

16. Hama, F. R.: "An Efficient Tripping Device". *Journal of the Aeronautical Sciences,* Volume 24, pp. 236-237, 1957.

17. Hegarty, J. C. and Hama, F. R.: *Further Investigation on the Triangular Patch Stimulator.* University of Maryland Technical Note BN-107, AFOSR TN-57-616, ASTIA AD 136 605, 1957.

18. Schlichting, H.: *Boundary Later Theory,* 7th edition. McGraw-Hill, pp. 168-173, 1979.

19. Rao, D. M.: "Side-Force Alleviation on Slender, Pointed Forebodies at High Angles of Attack". *Journal of Aircraft,* Volume 16, Number 11, pp. 763-768, 1979.

20. Carr, P. C. and Gilbert, W. P.: *Effects of Fuselage Forebody Geometry on Low-Speed Lateral-Directional Characteristics of Twin-Tail Fighter Model at High Angles of Attack.* NASA TP 1592, 1979.

21. Ralston, J. N.: *Rotary Balance Data and Analysis for the X-29A Airplane for an Angle-of-Attack Range of 0° to 90.* NASA CR 3747, 1984.

Table 1. Dimensional Characteristics of the X-29A Airplane

Overall length, ft	48.0
Wing:	
Span, ft	27.2
Reference area, ft^2	185.0
Exposed area, ft^2	160.0
Mean aerodynamic chord, in	86.6
Aspect ratio	4.0
Taper ratio	0.4
Leading-edge sweep, deg	-29.27
Quarter-chord sweep, deg	-33.73
Airfoil section:	
Root thickness, percent chord	6.7
Tip thickness, percent chord	6.0
Canards:	
Span, ft	13.6
Reference area (total), ft^2	37.0
Exposed area (total), ft^2	36.49
Aspect ratio	1.47
Taper ratio	0.319
Leading-edge sweep, deg	42.0
Quarter-chord sweep, deg	23.08
Airfoil section:	
Root thickness, percent chord	5.0
Tip thickness, percent chord	3.5
Vertical stabilizer:	
Reference area, ft^2	34.0
Aspect ratio	2.68
Taper ratio	0.30
Leading-edge sweep, deg	47.0
Airfoil section:	
Root thickness, percent chord	4.0
Tip thickness, percent chord	4.0

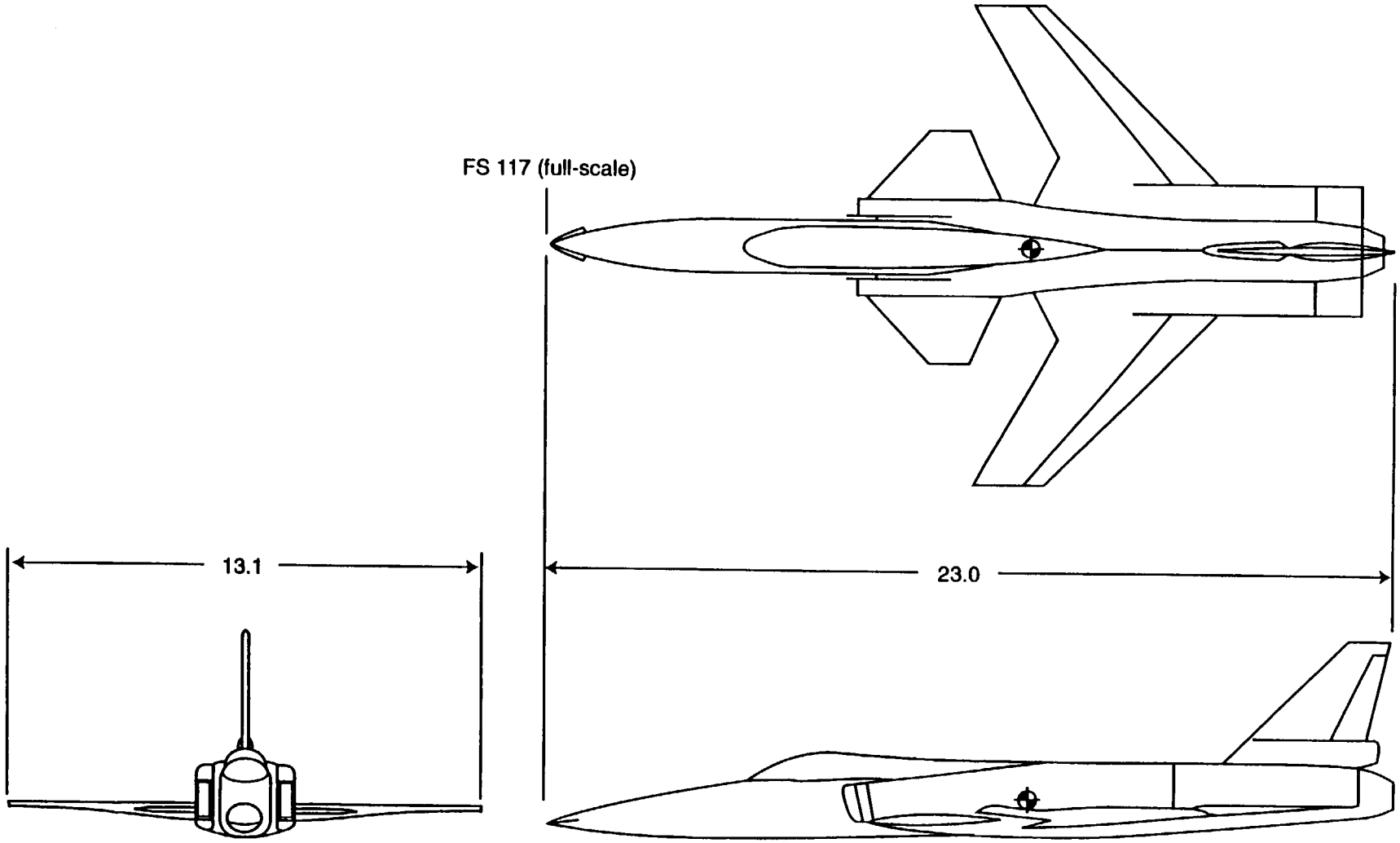

Figure 1. Three-view sketch of baseline 1/25 - scale model. Moment reference point shown is FS 454.27 (-0.05$\bar{c}$),WL 66, BL 0. (Dimensions are in inches.)

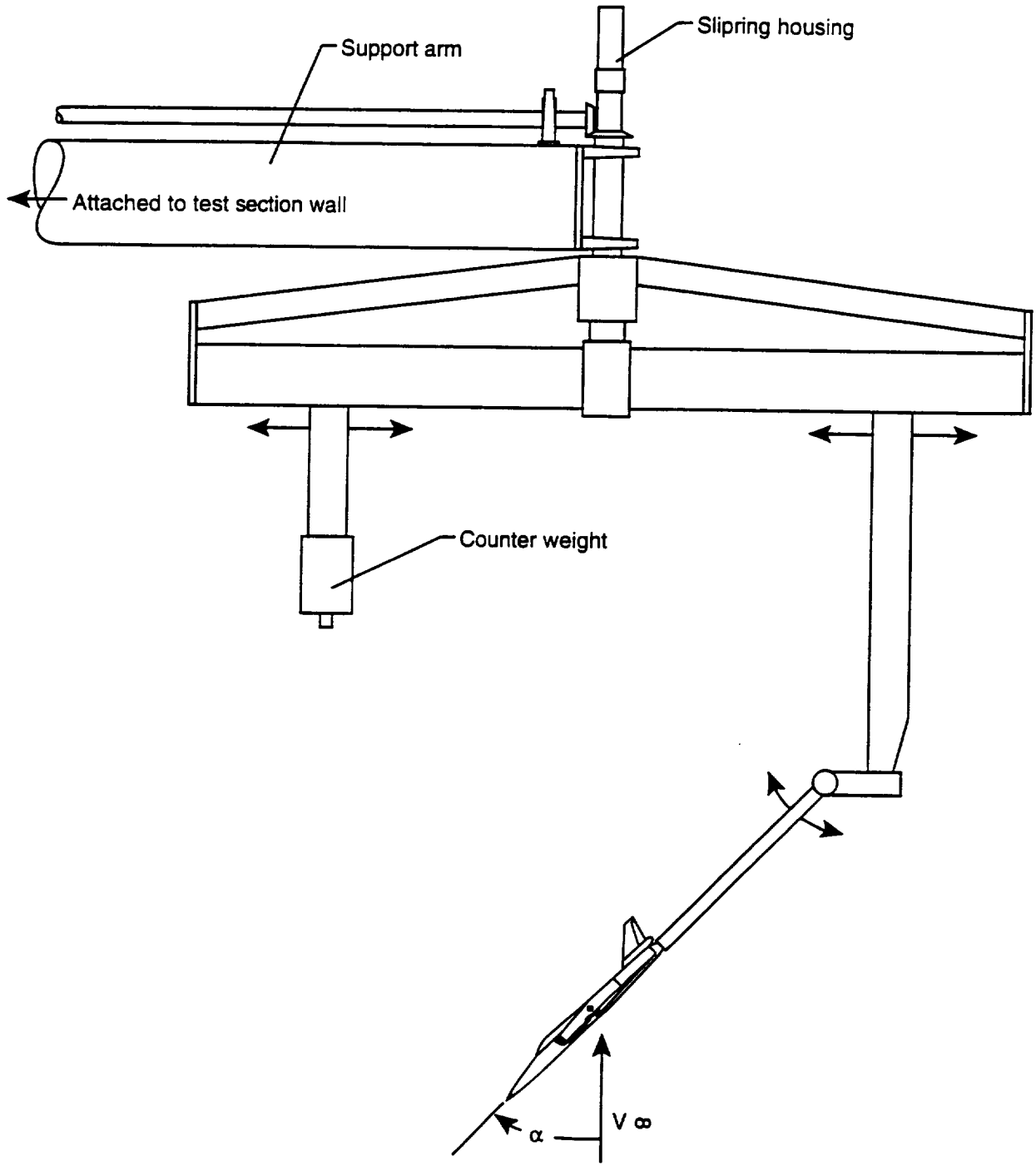

a. Angle of attack definition.

Figure 2. Sketch of 1/25 - scale X-29A model mounted on 20-foot Vertical Spin Tunnel rotary balance for static testing.

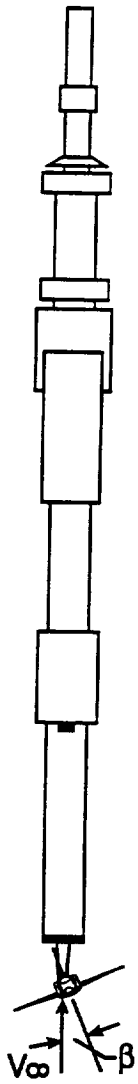

b. Sideslip angle definition at α =90°.

Figure 2. Concluded.

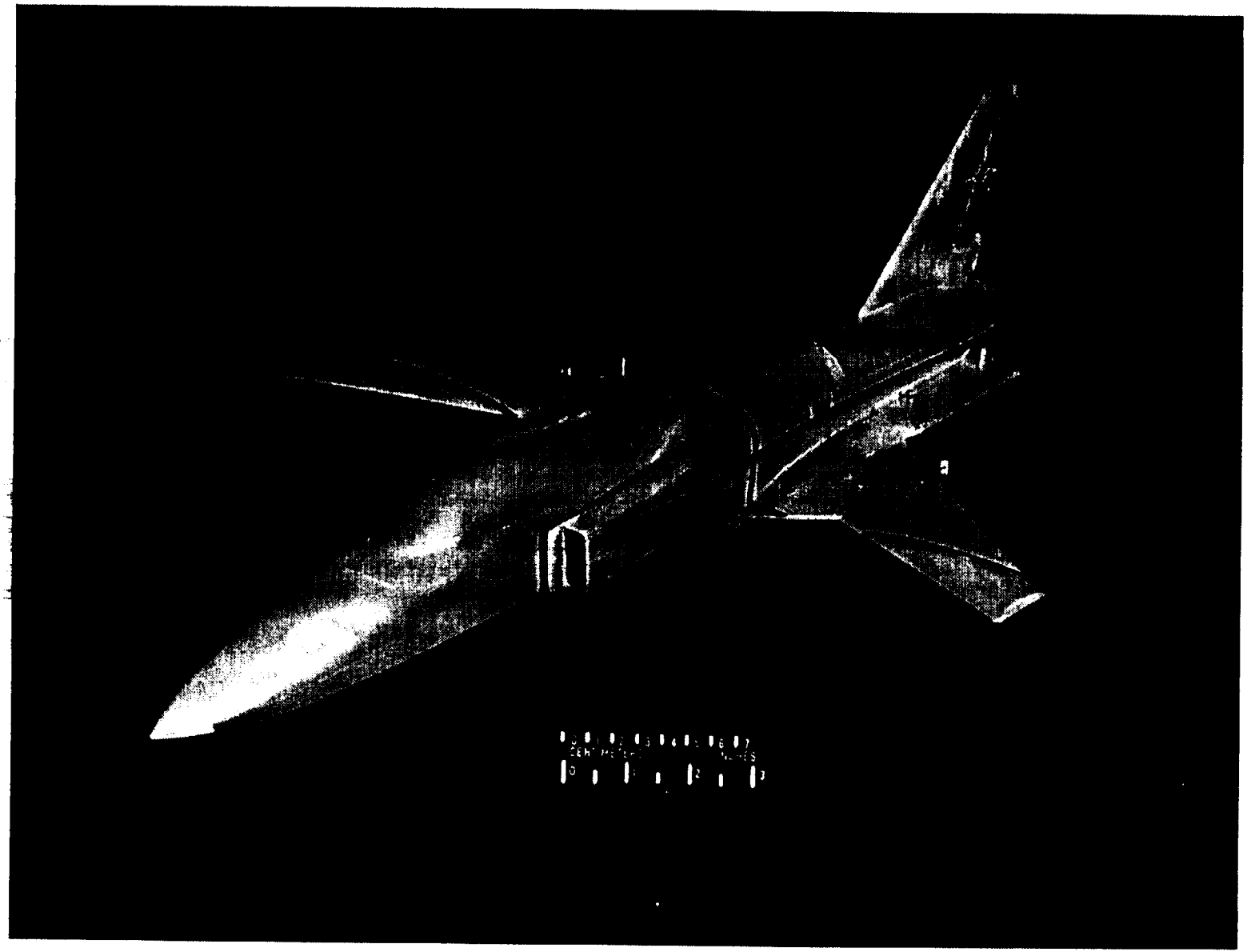

Figure 3. Photograph of baseline 1/25-scale model.

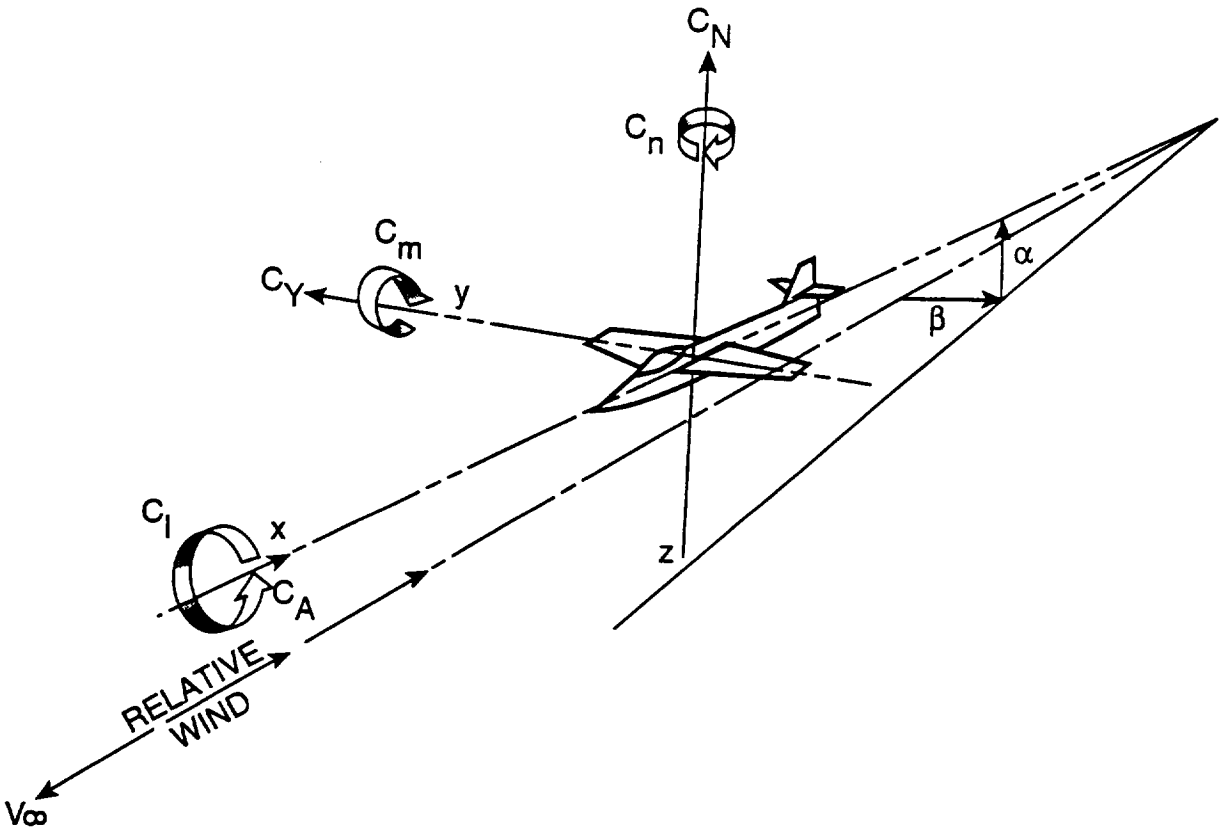

Figure 4. Orientation of force and moment coefficients about body axes. Positive directions of force coefficients, moment coefficients, and angles are indicated by arrows.

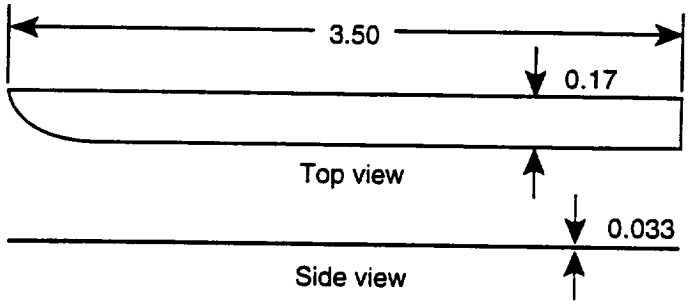

a. Strake 1.

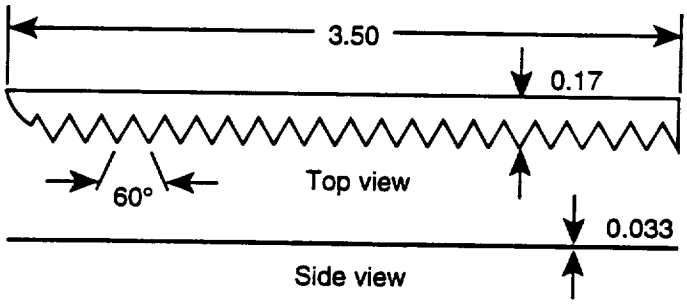

b. Strake 2.

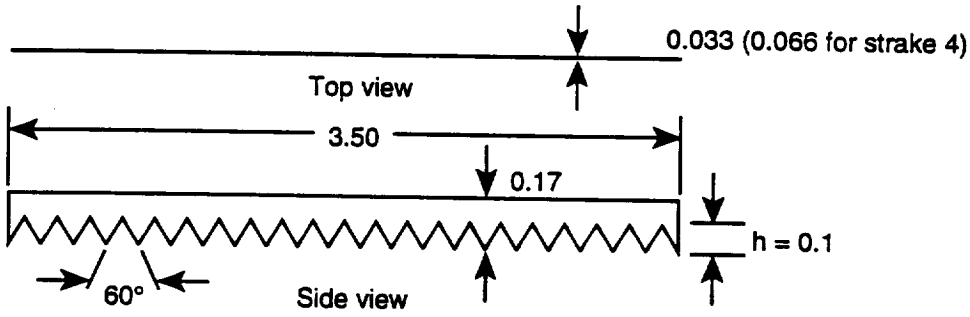

c. Strakes 3 and 4.

Figure 5. Forebody strakes 1 through 4. Linear dimensions are in inches.

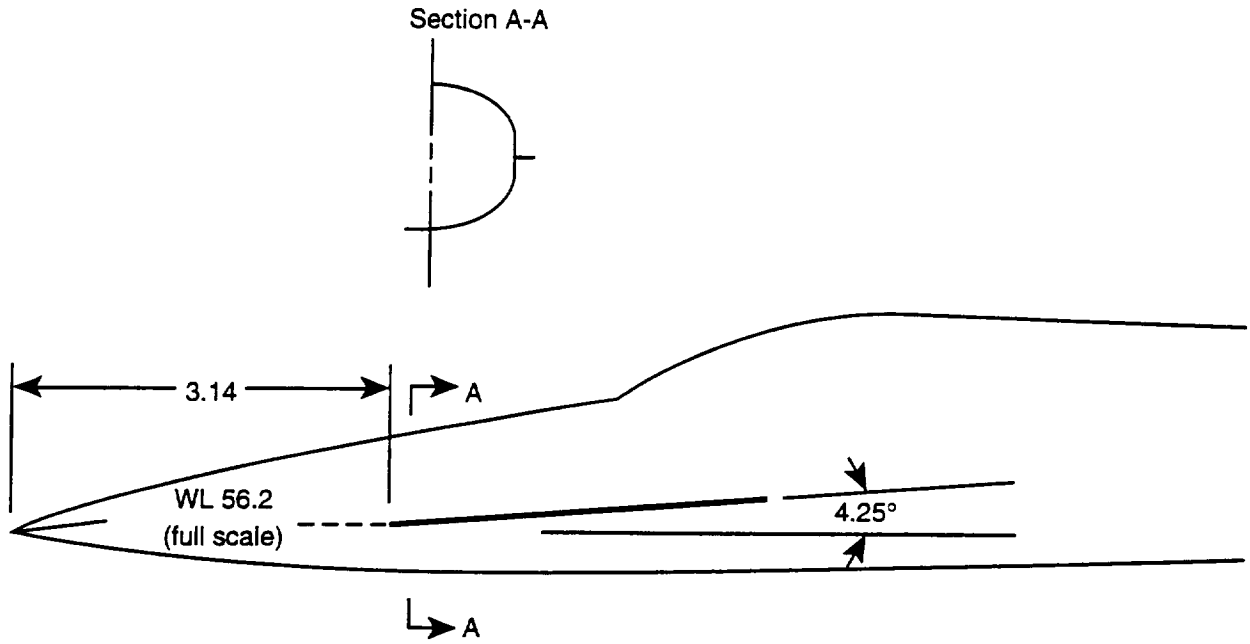

a. Strakes 1 and 2.

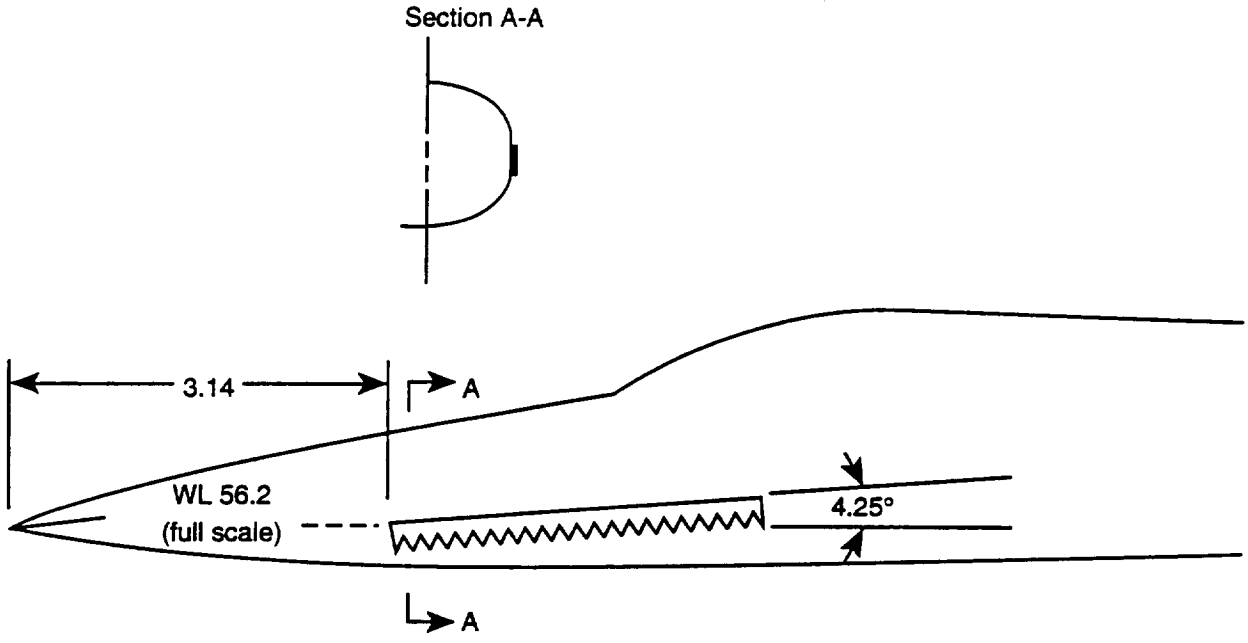

b. Strakes 3 and 4.

Figure 6. Placment of forebody strakes 1 through 4 on X-29A model. Linear dimensions are in inches.

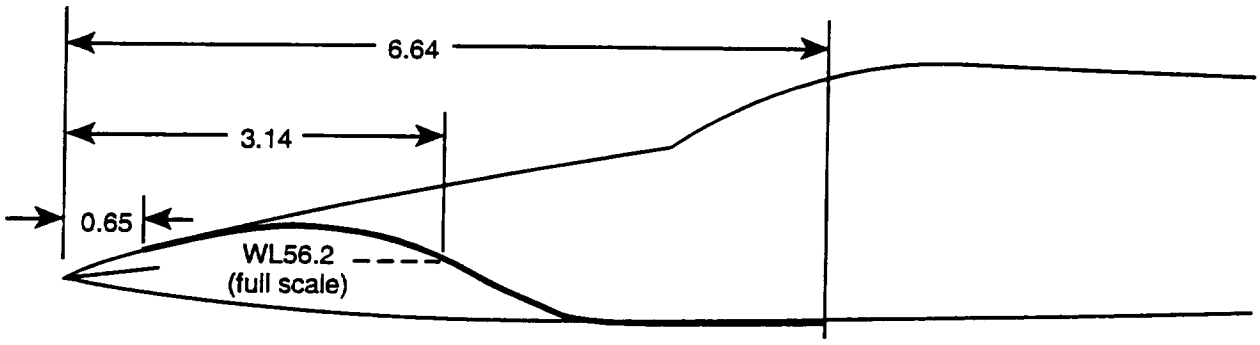

a. Side view.

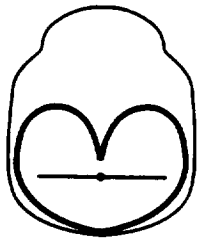

b. Front view.

Figure 7. General arrangement of helical trip wire on forebody of the X-29A model. Dimensions are in inches.

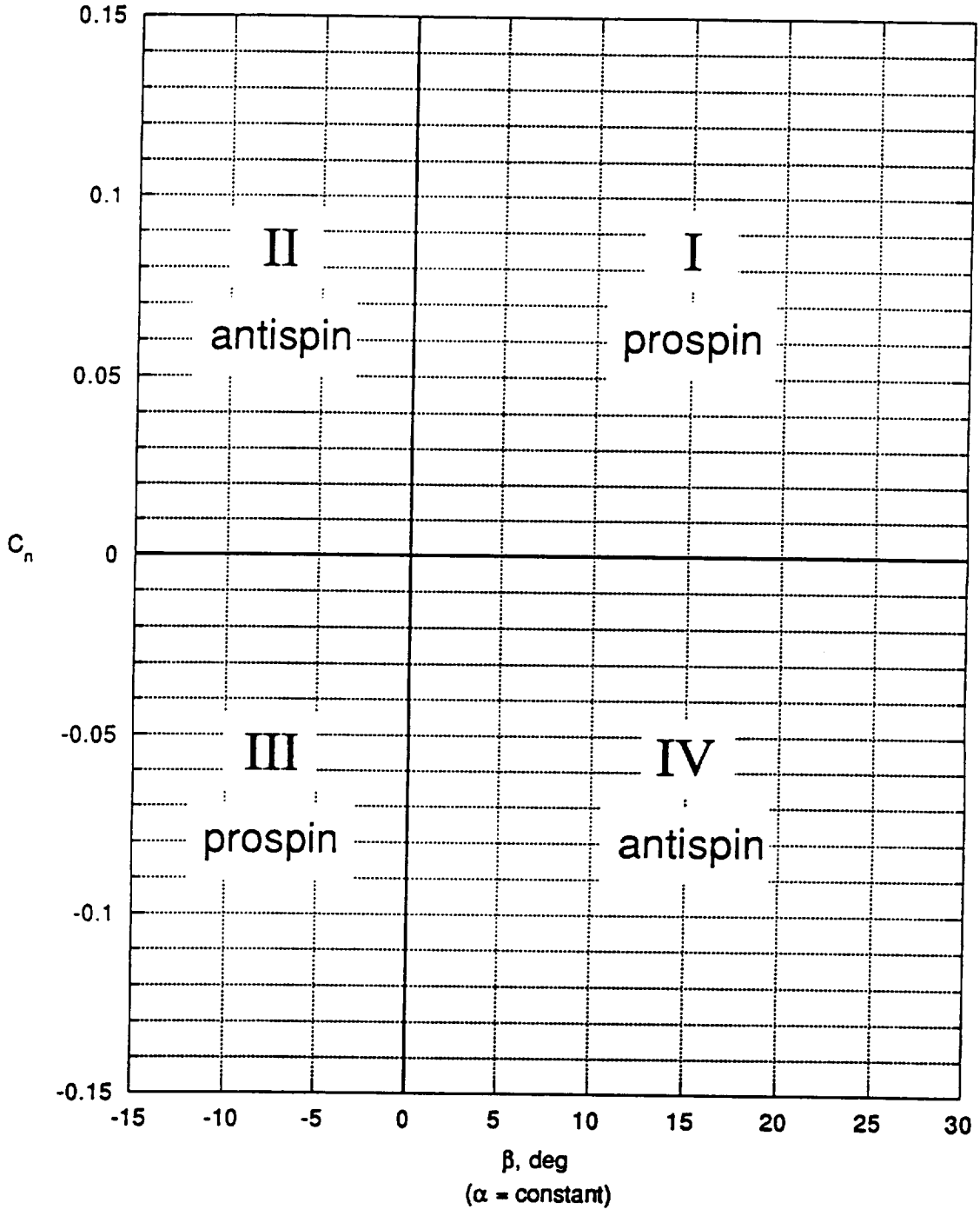

Figure 8. Illustration of prospin and antispin quadrants of C_n- vs.- β plots used for analysis of static data at spinning attitudes.

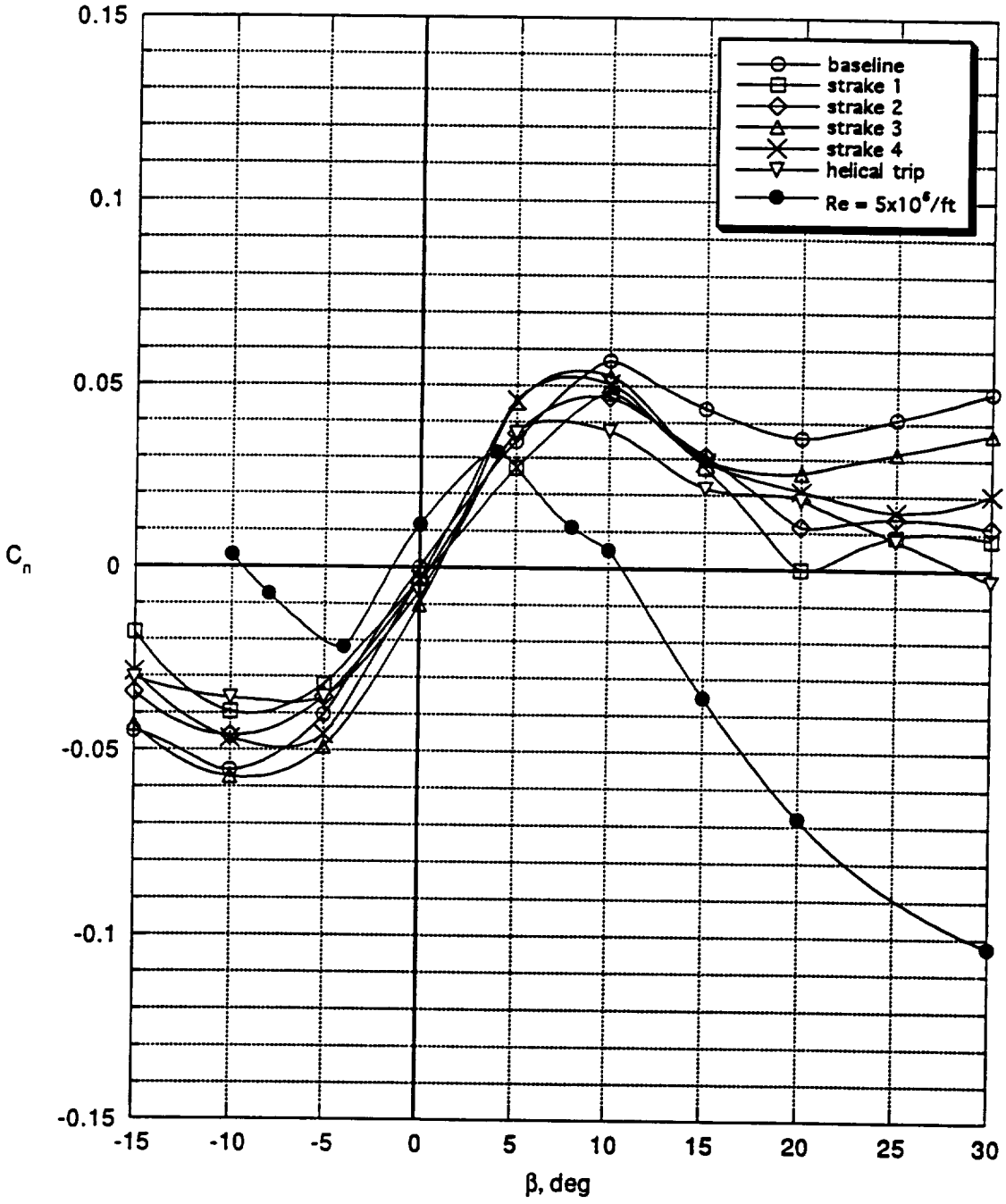

(a) $\alpha = 40°$.

Figure 9. Static yawing moment characteristics of the X-29A at low- and high-Reynolds numbers, including the effects of forebody modifications. Angle of attack is constant.

(δ_c=-60°, δ_a=25°, δ_s=30°, δ_r=0°)

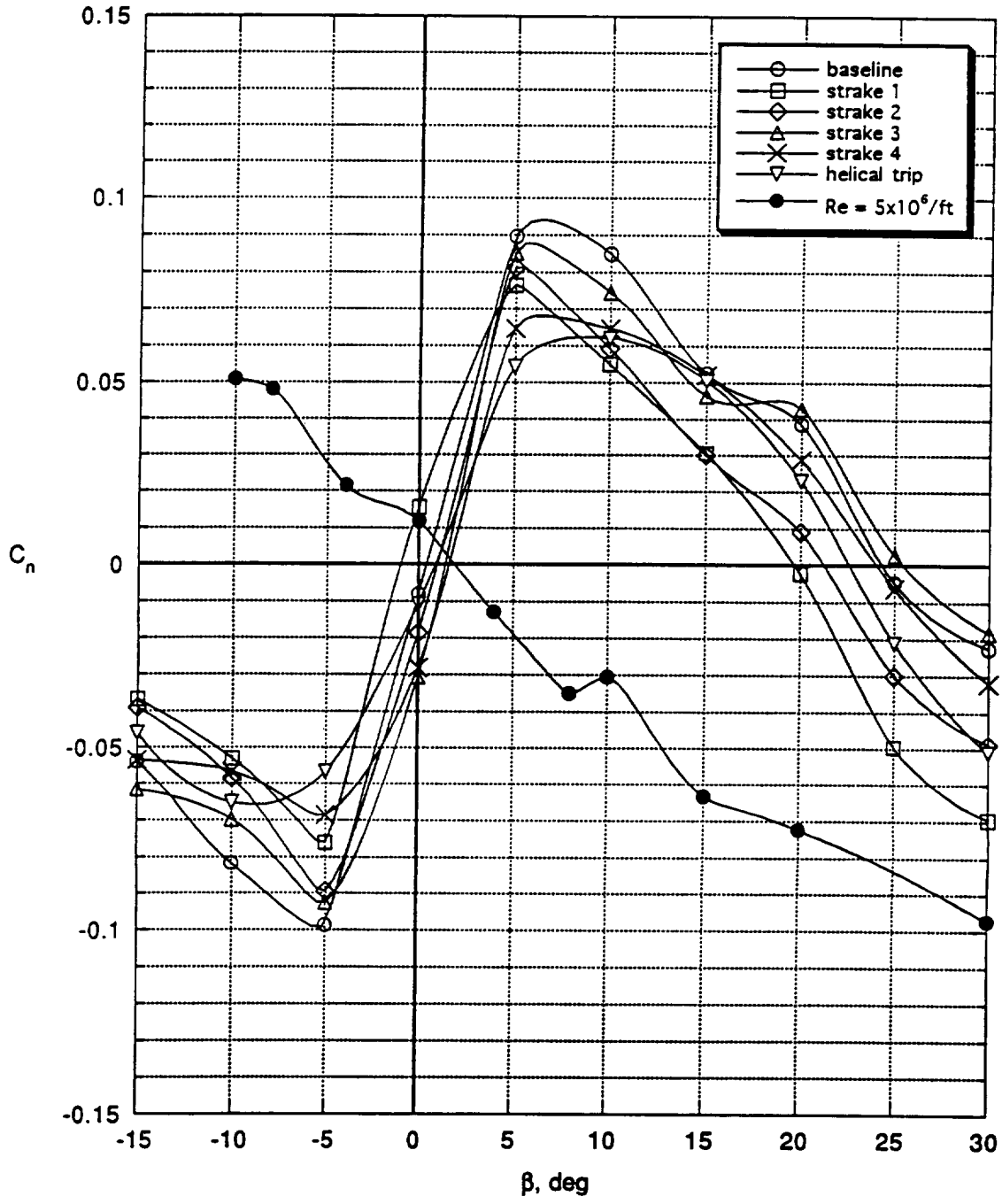

(b) $\alpha = 50°$.

Figure 9. Continued.

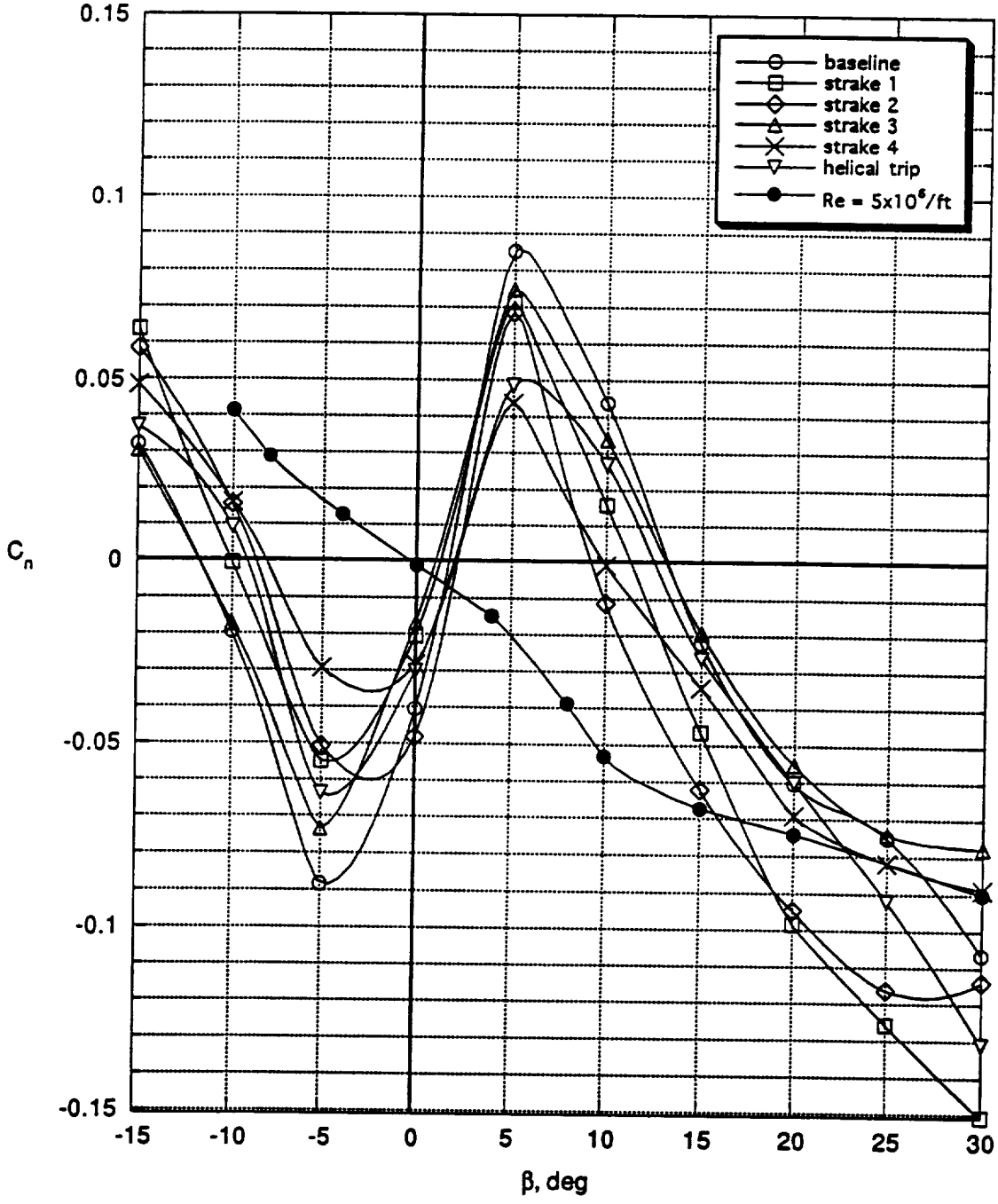

(c) $\alpha = 60°$.

Figure 9. Continued.

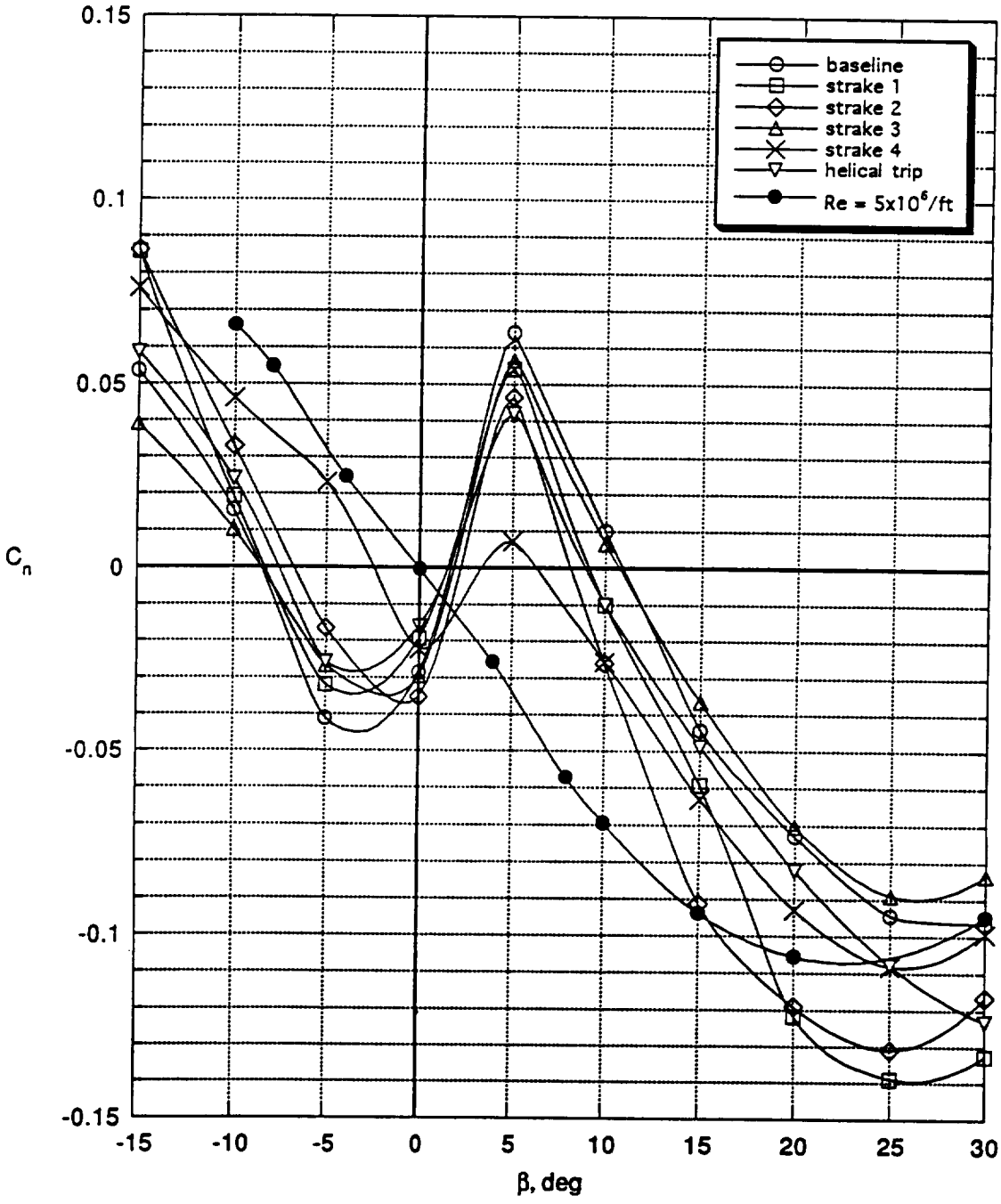

(d) $\alpha = 65°$.

Figure 9. Continued.

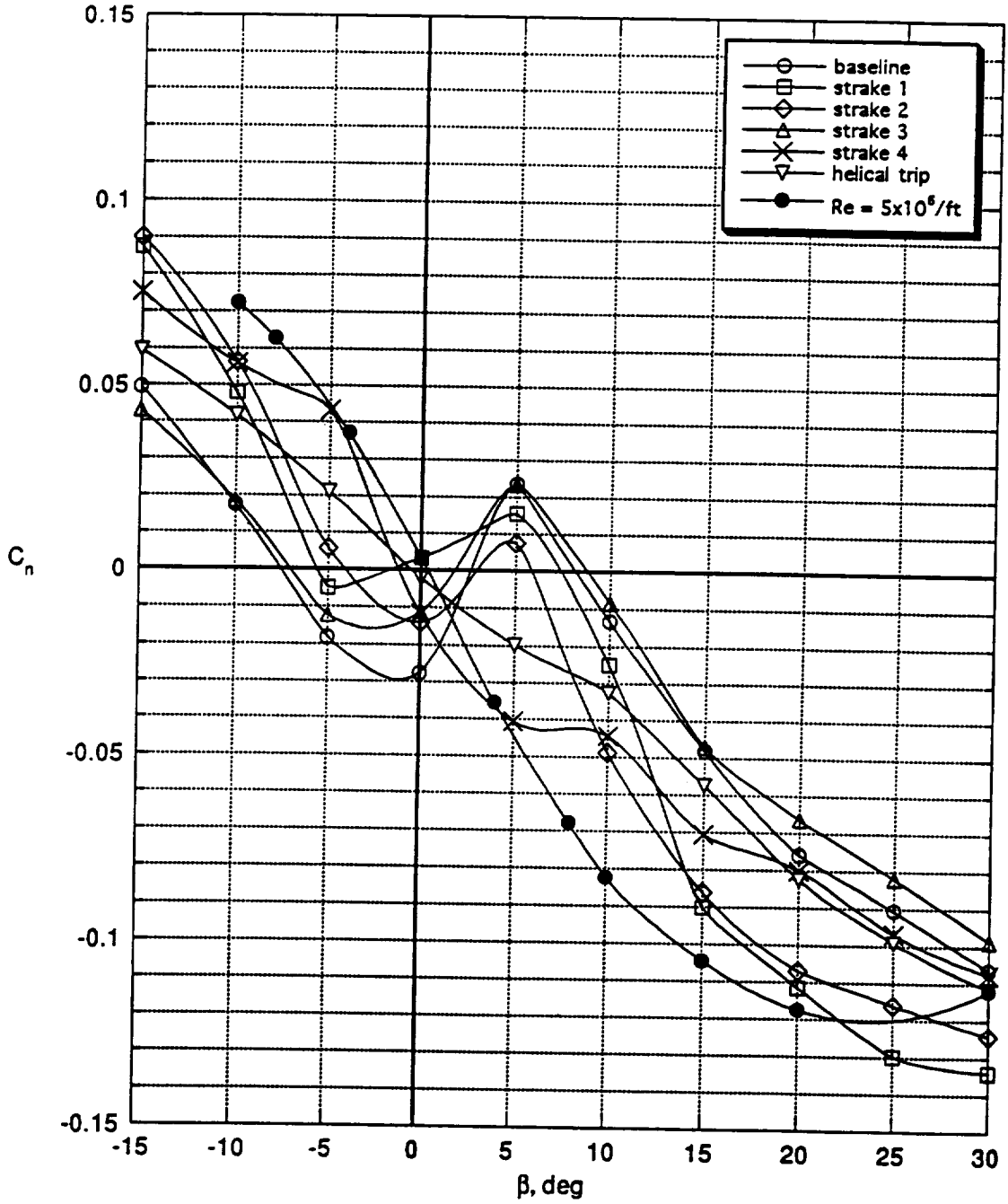

(e) $\alpha = 70°$.

Figure 9. Continued.

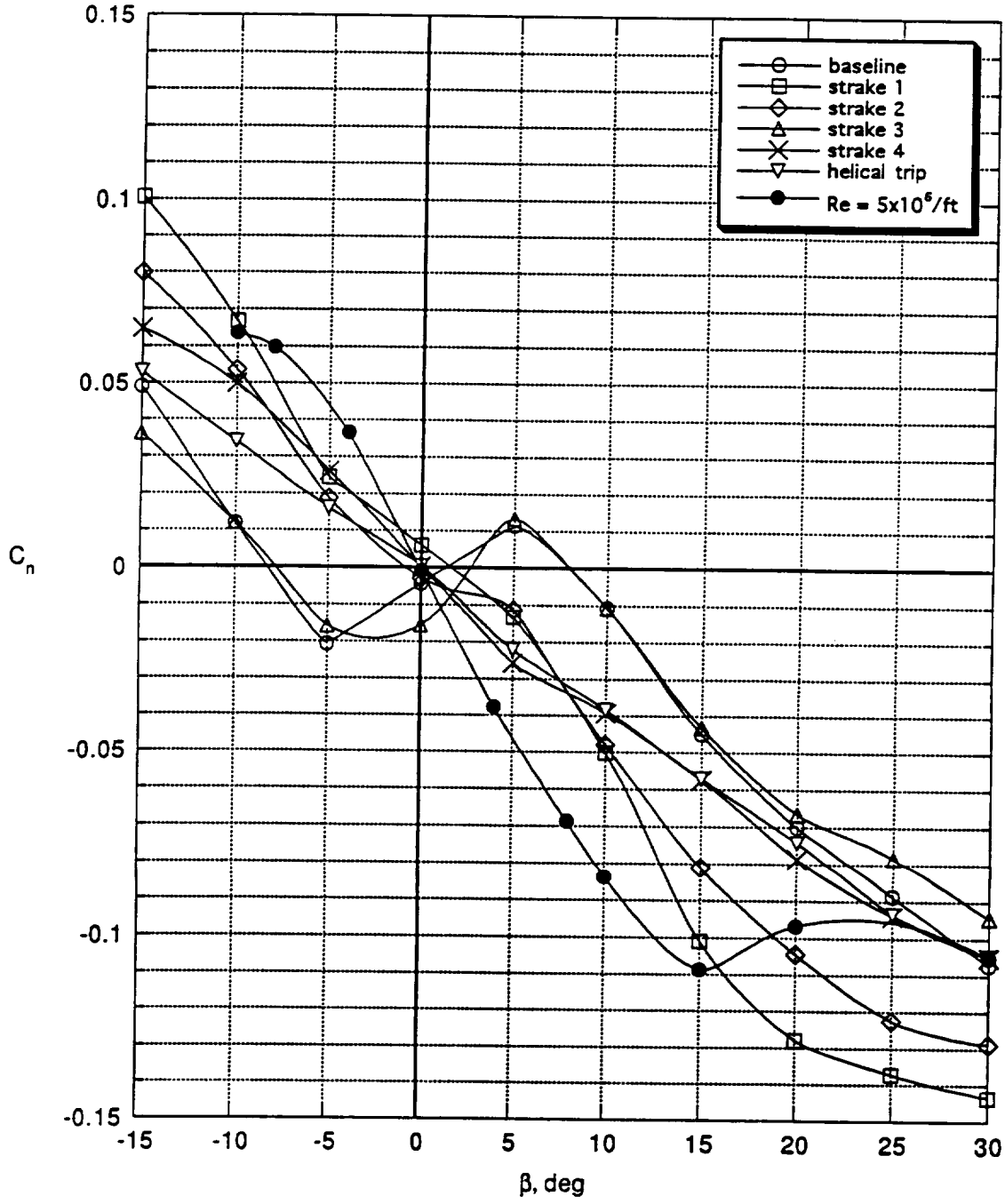

(f) $\alpha = 75°$.

Figure 9. Continued.

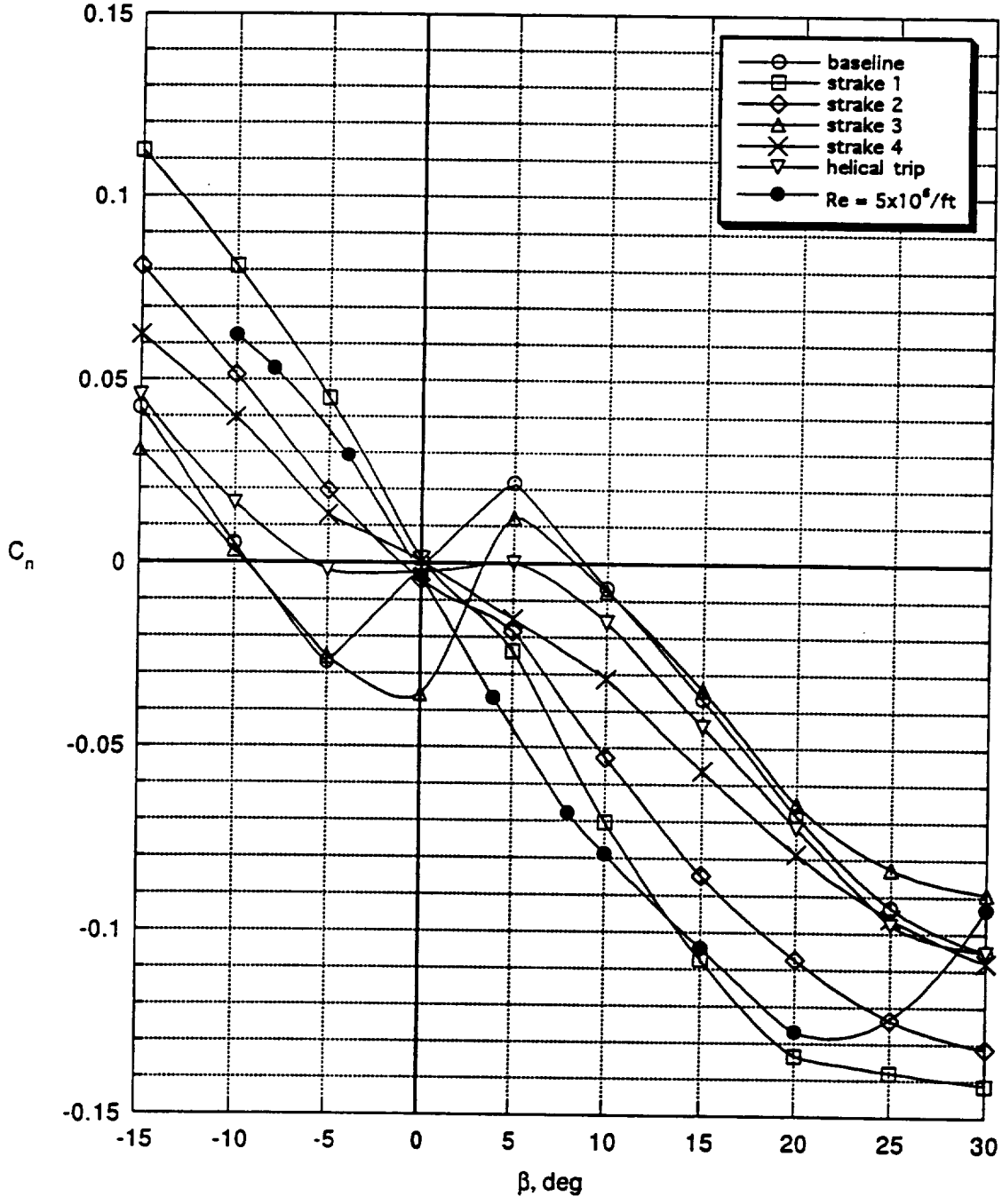

(g) $\alpha = 80°$.

Figure 9. Continued.

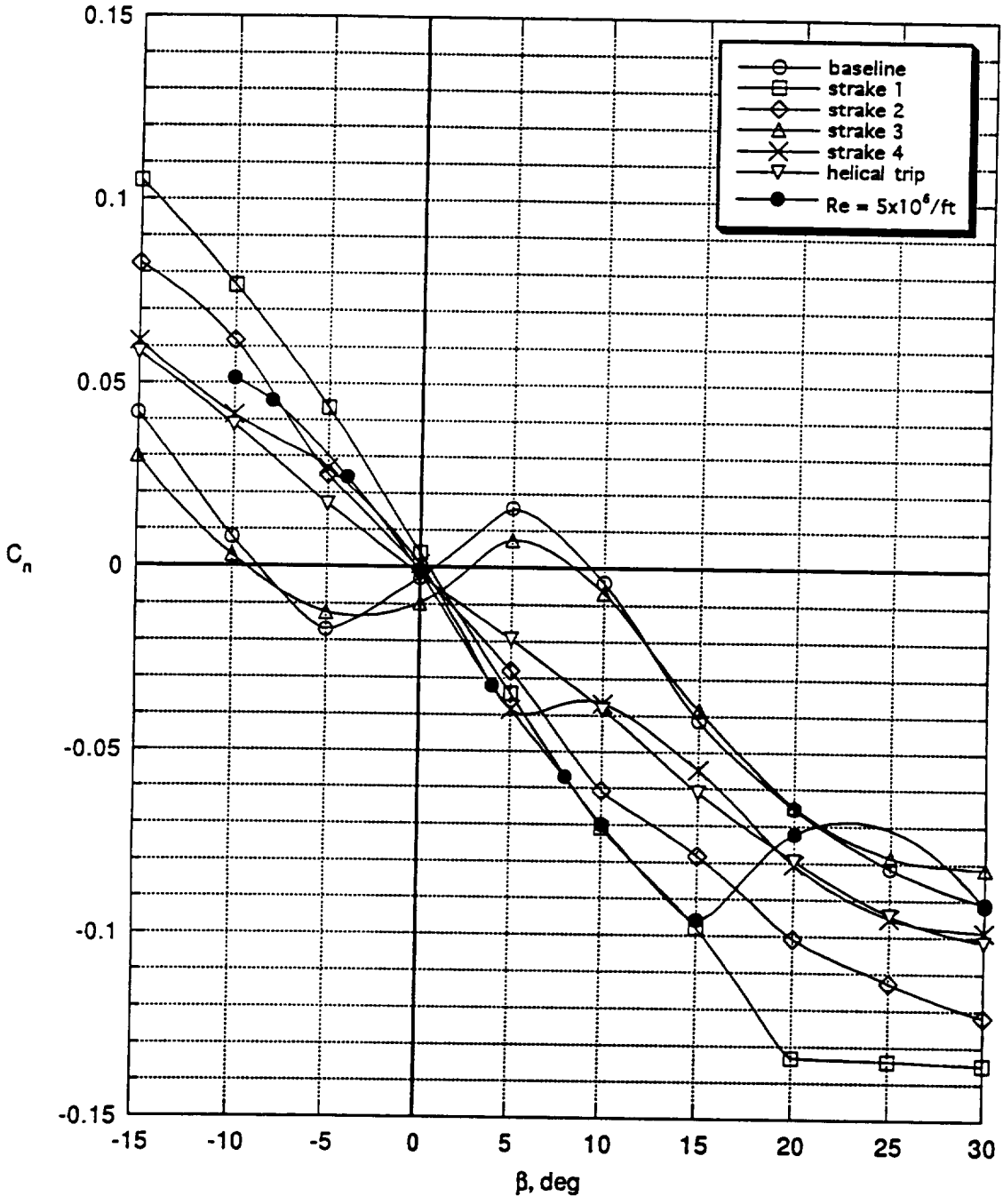

(h) $\alpha = 85°$.

Figure 9. Continued.

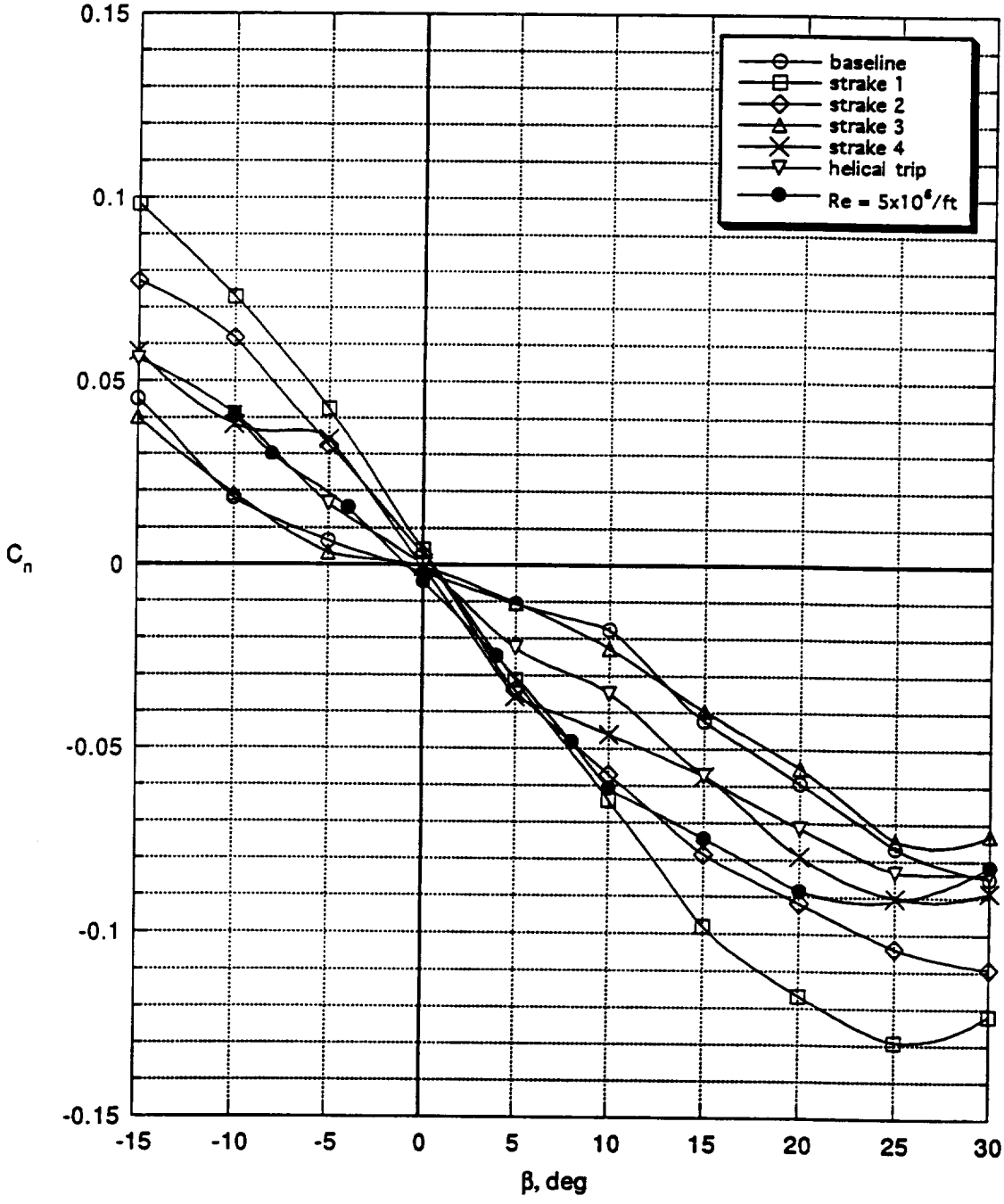

(i) $\alpha = 90°$.

Figure 9. Concluded.

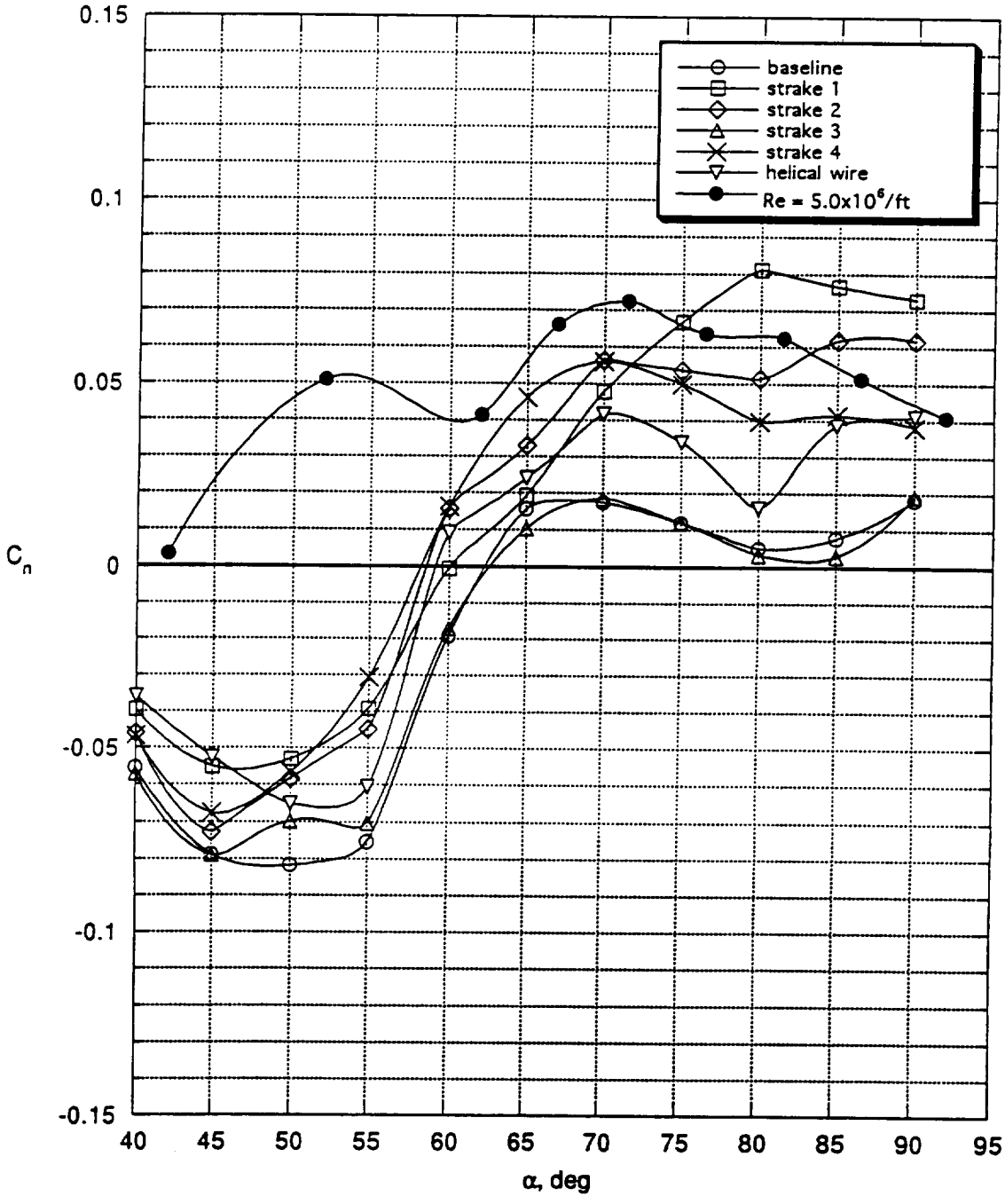

(a) $\beta = -10°$.

Figure 10. Static yawing moment characteristics of the X-29A at low- and high-Reynolds numbers, including the effects of forebody modifications. Sideslip angle is constant.

(δ_c=-60°, δ_a=25°, δ_s=30°, δ_r=0°)

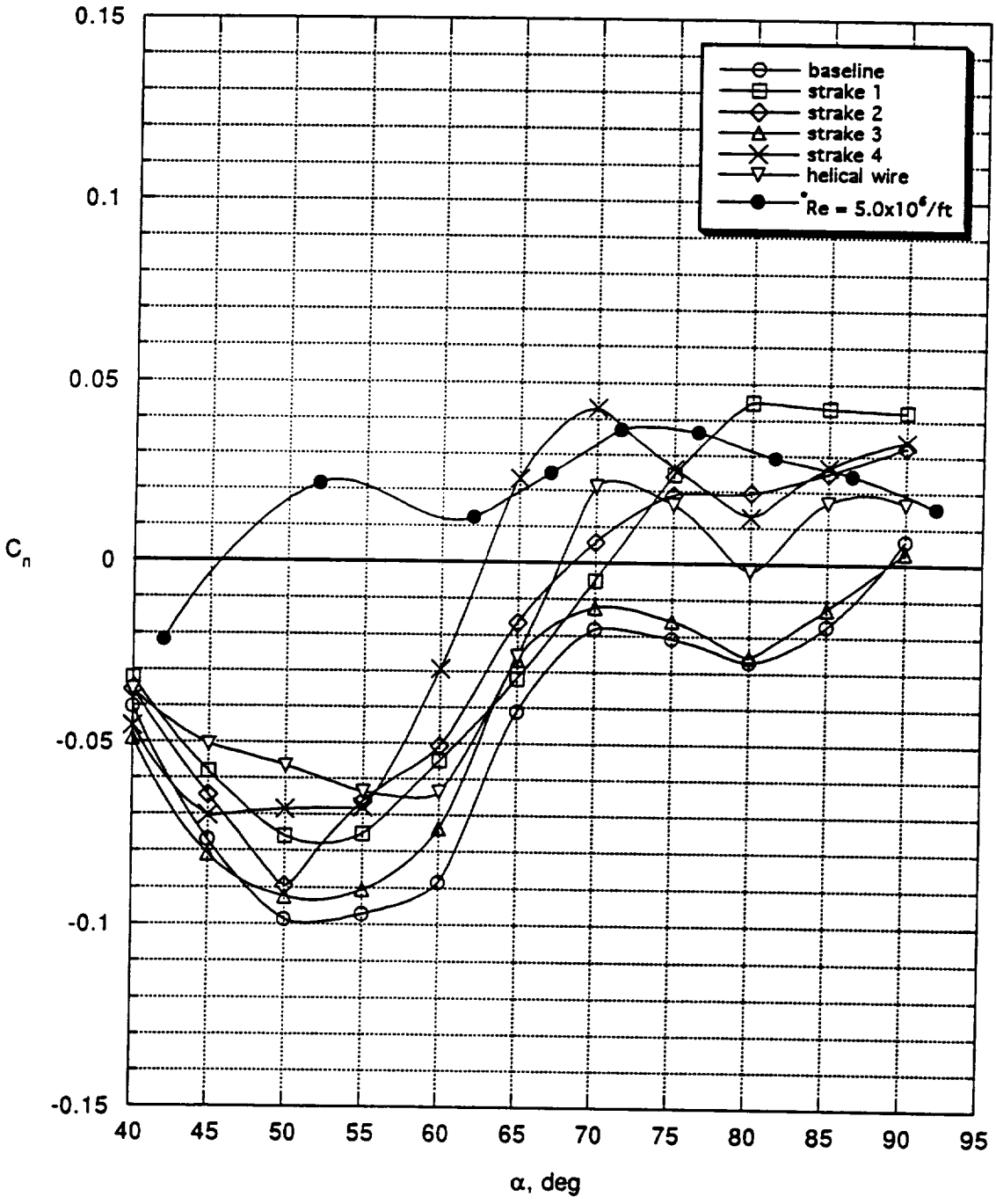

(b) $\beta = -5^\circ$ ($^*\beta = -4^\circ$ for Re = 5.0x10^6/ft).

Figure 10. Continued.

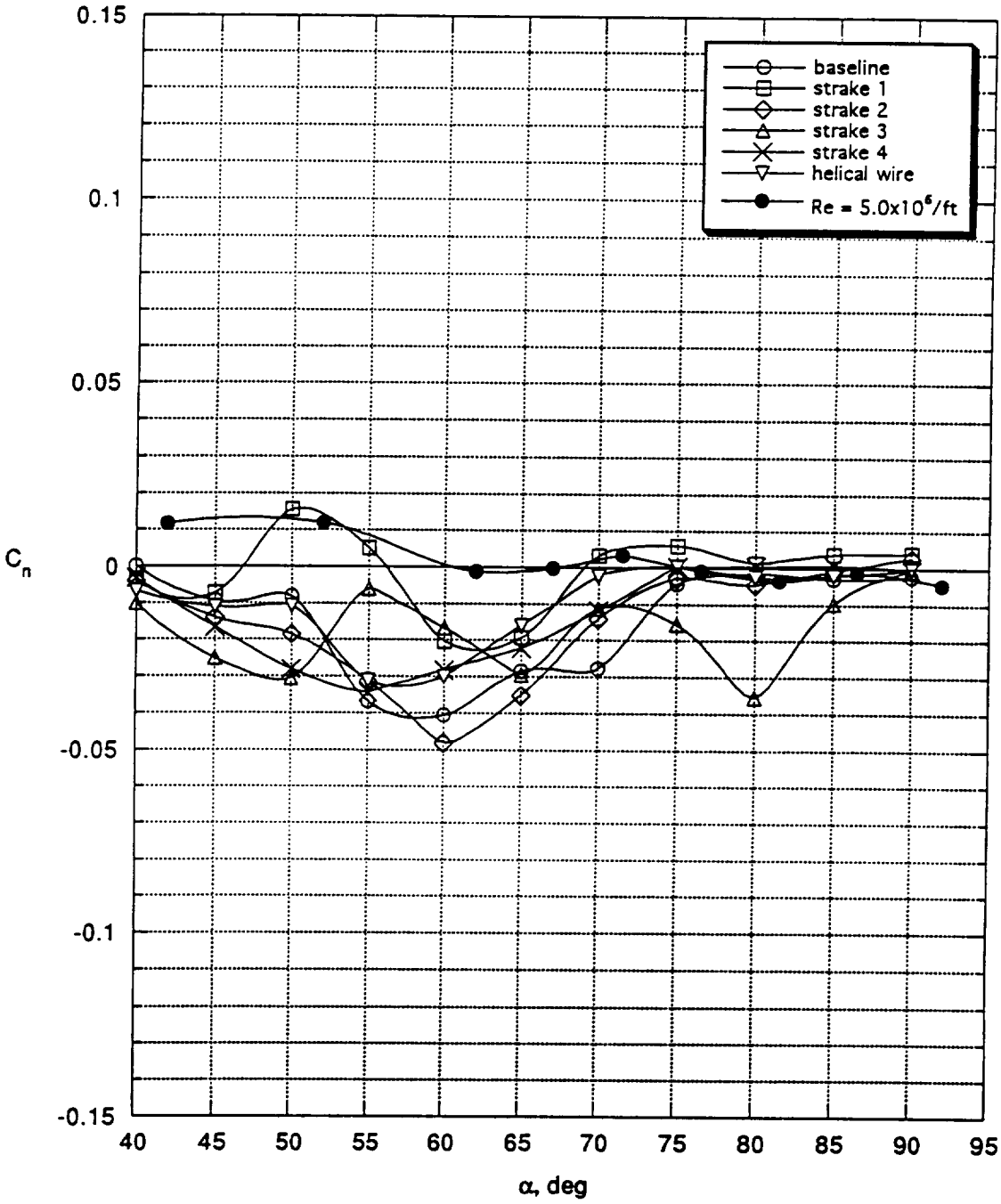

(c) $\beta = 0°$.

Figure 10. Continued.

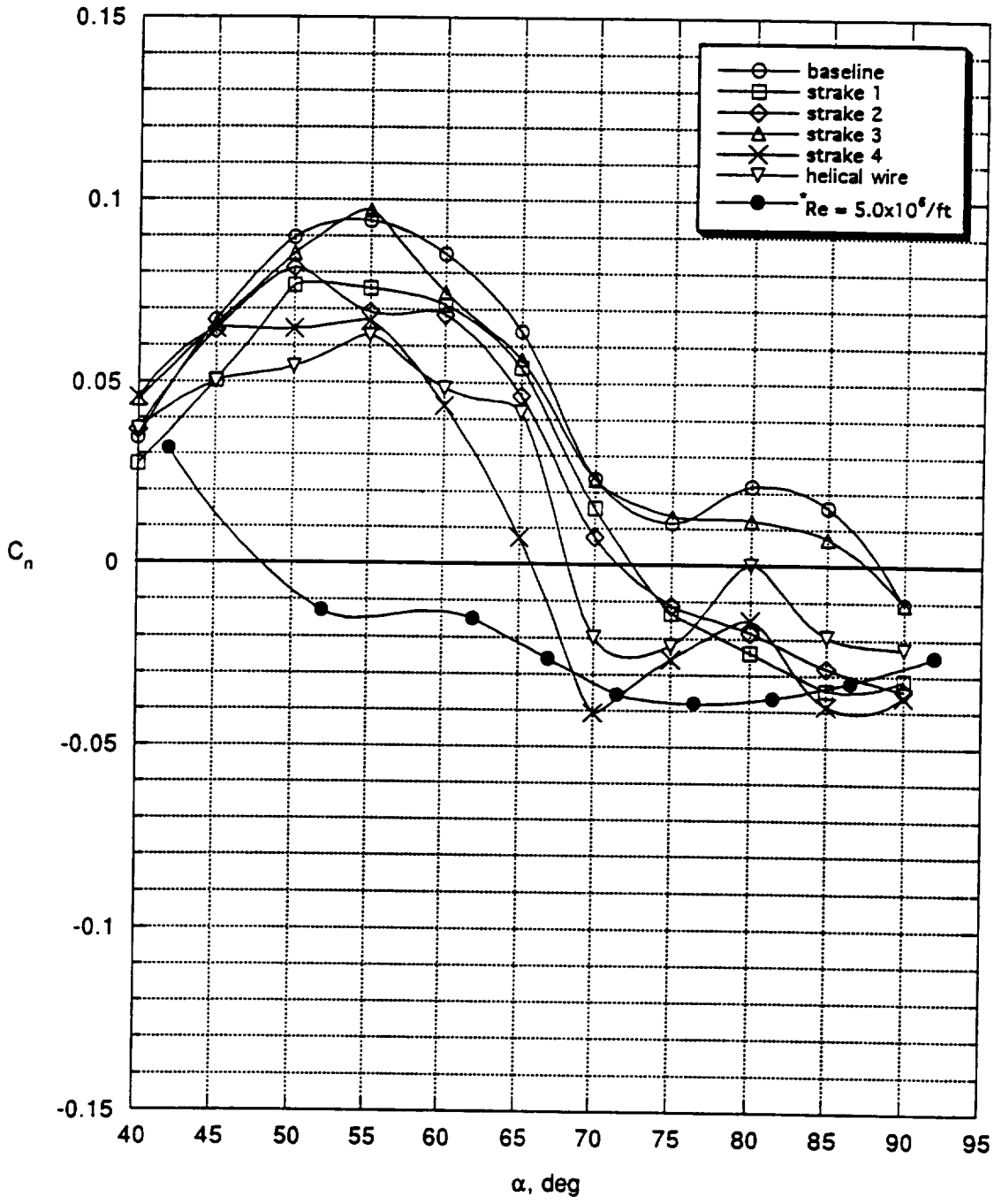

(d) $\beta = 5^\circ$ ($^*\beta = 4^\circ$ for Re = 5.0x10^6/ft).

Figure 10. Continued.

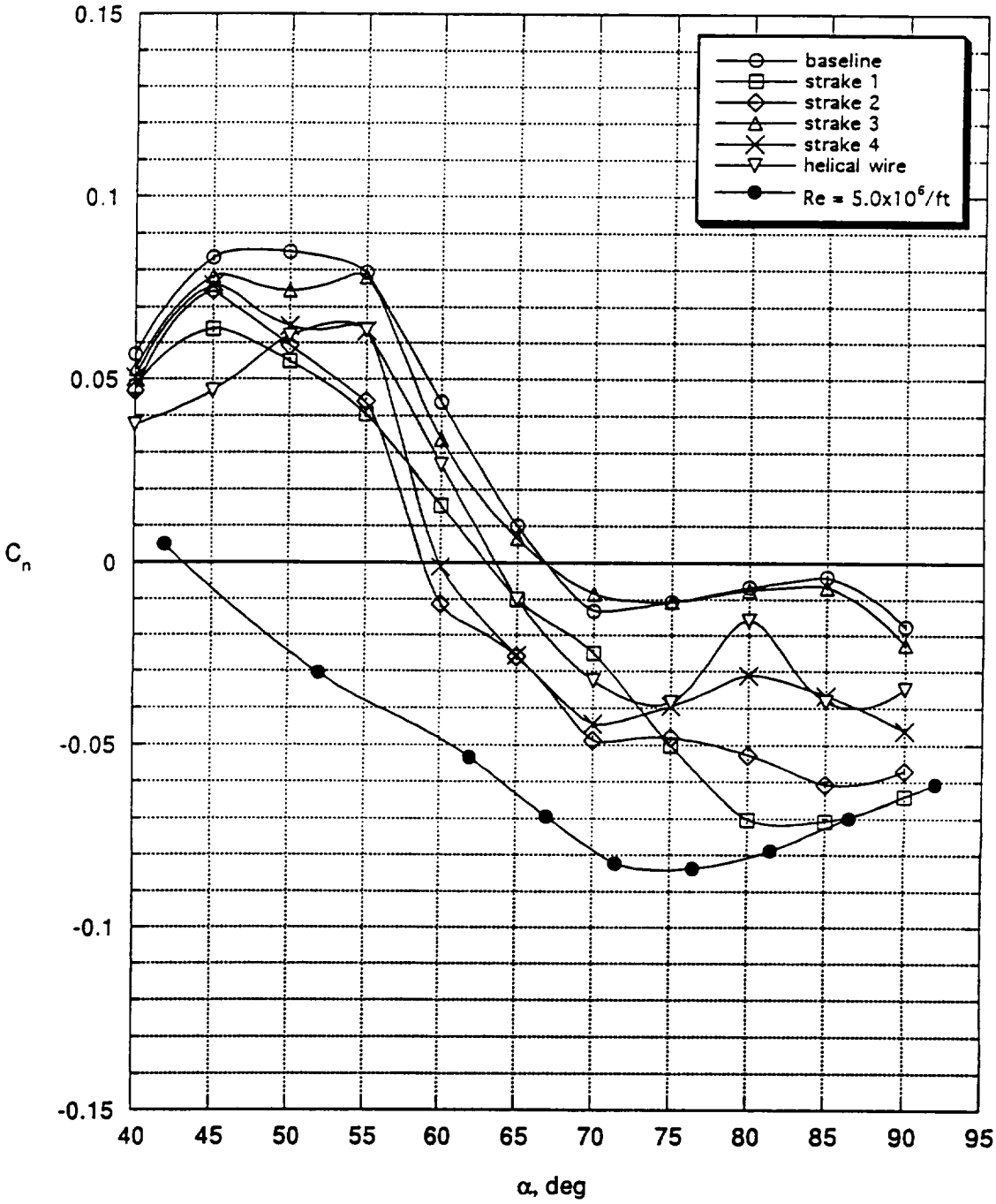

(e) $\beta = 10°$.

Figure 10. Continued.

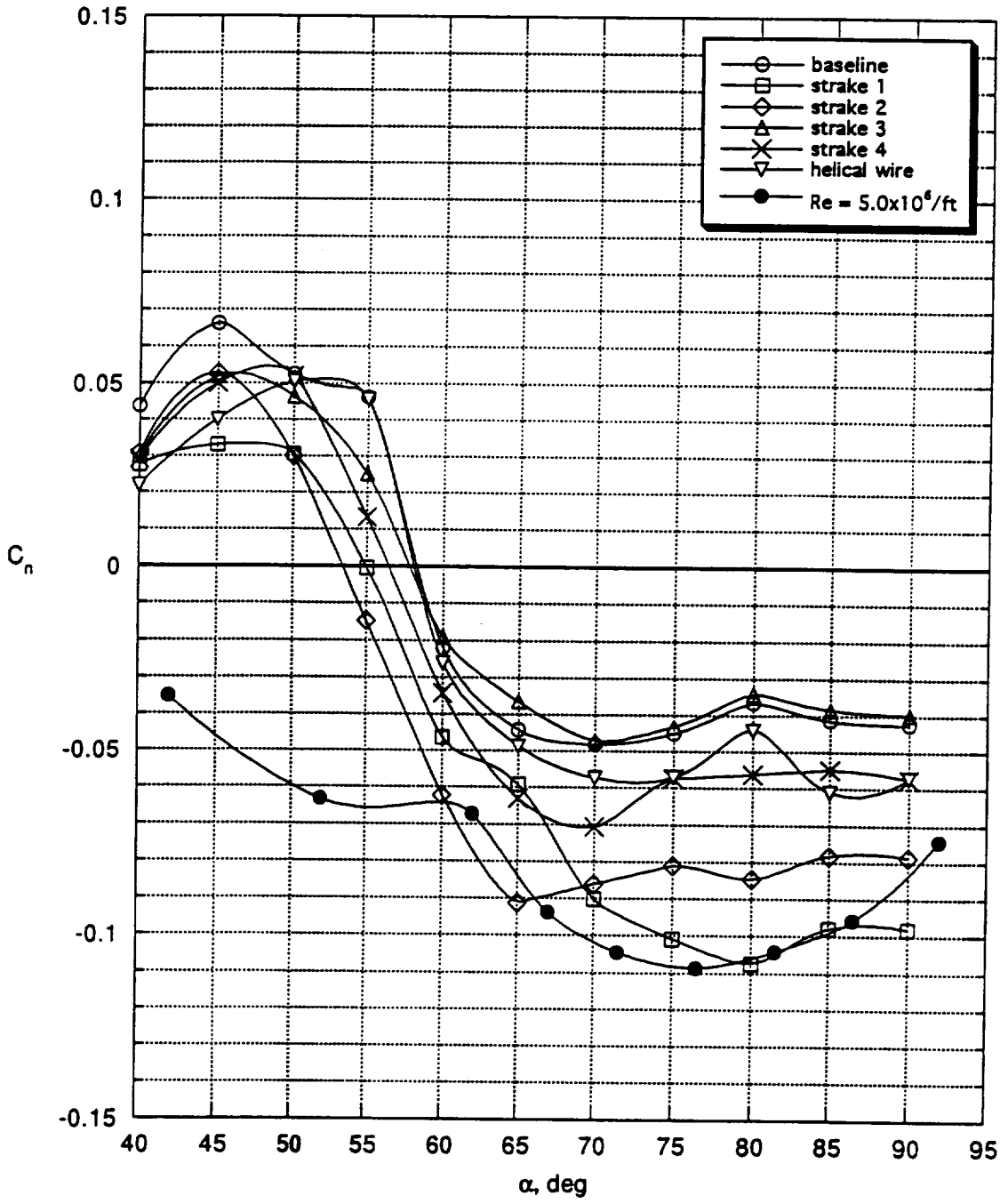

(f) $\beta = 15°$.

Figure 10. Continued.

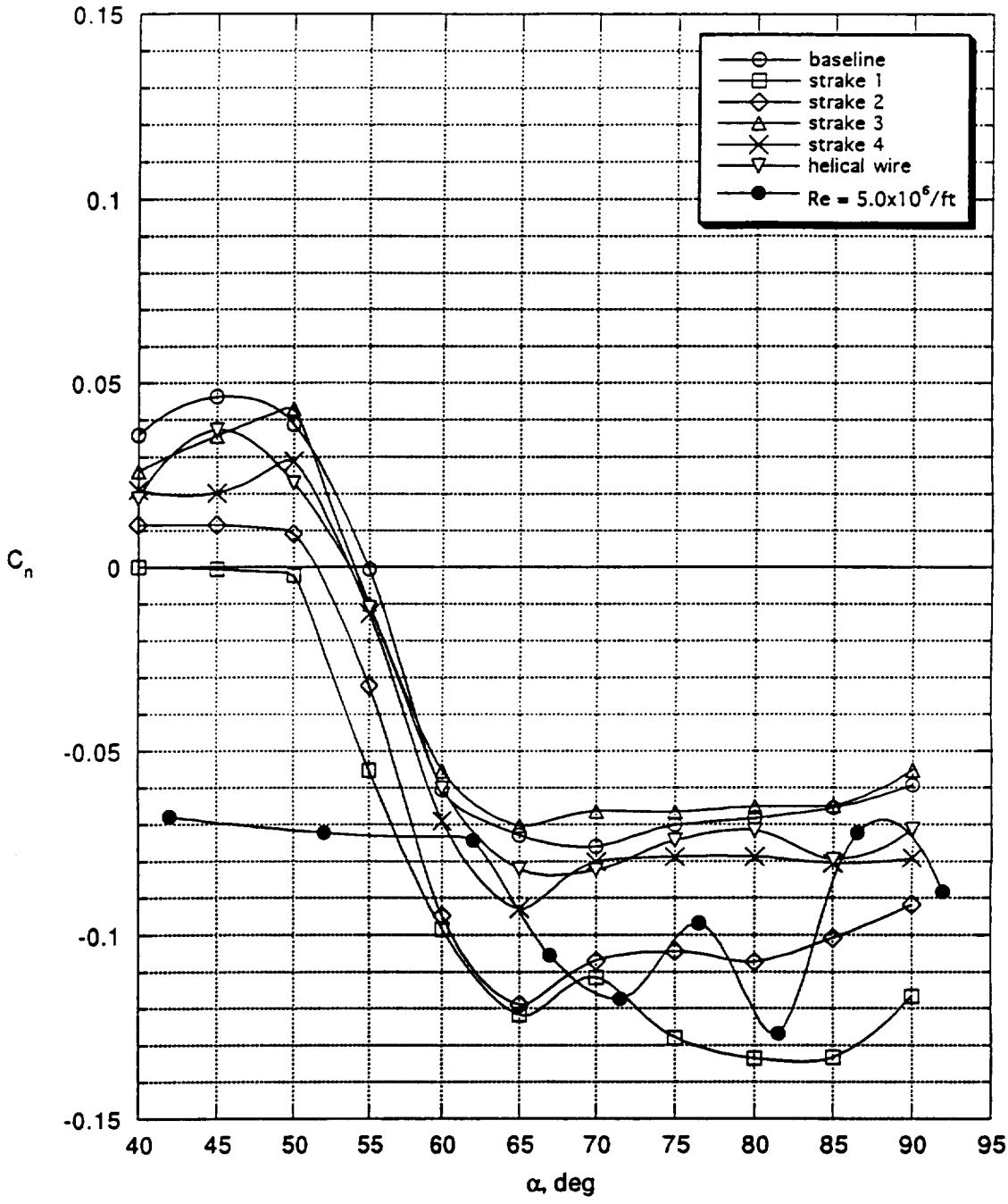

(g) $\beta = 20°$.

Figure 10. Continued.

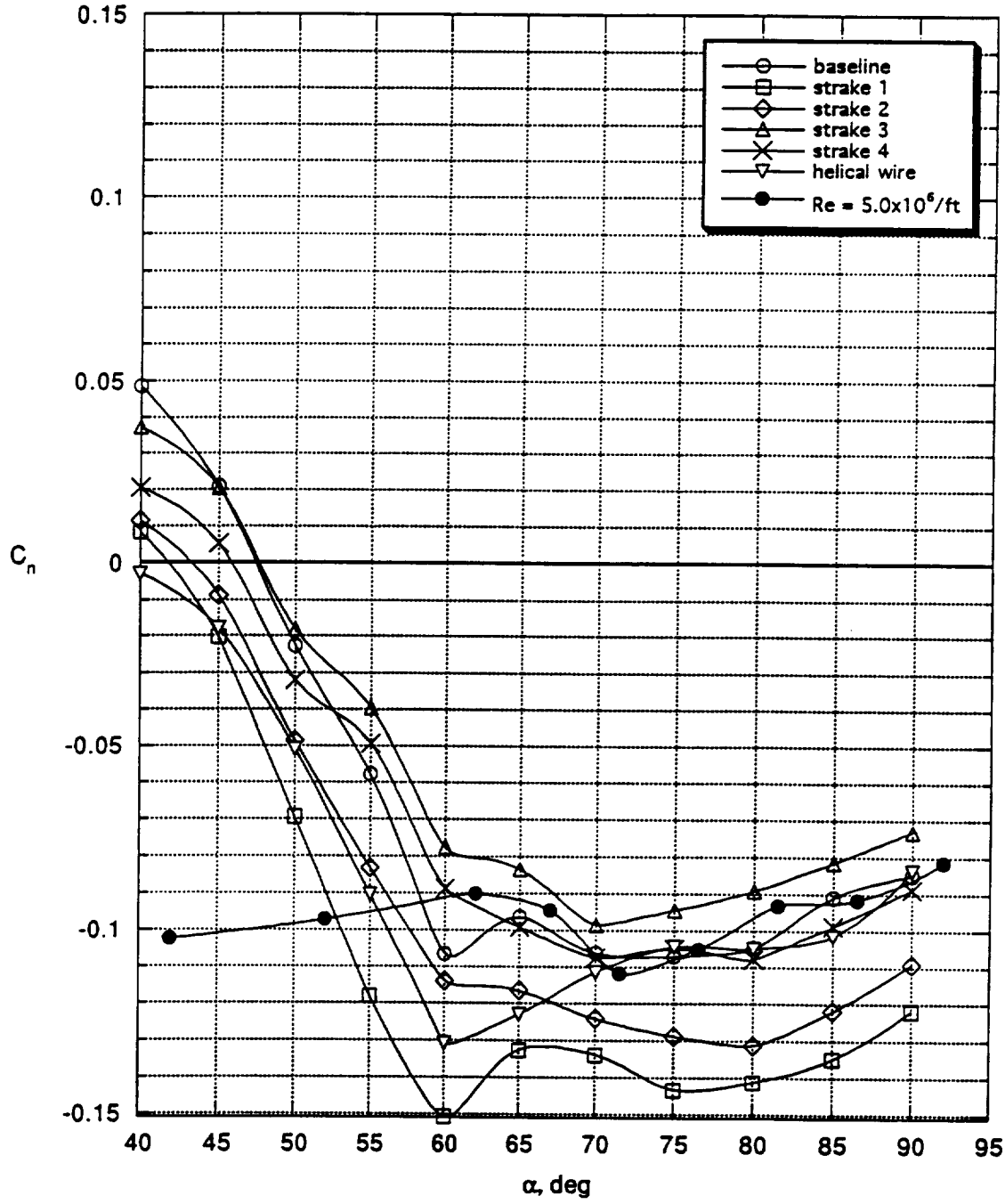

(h) $\beta = 30°$.

Figure 10. Concluded.

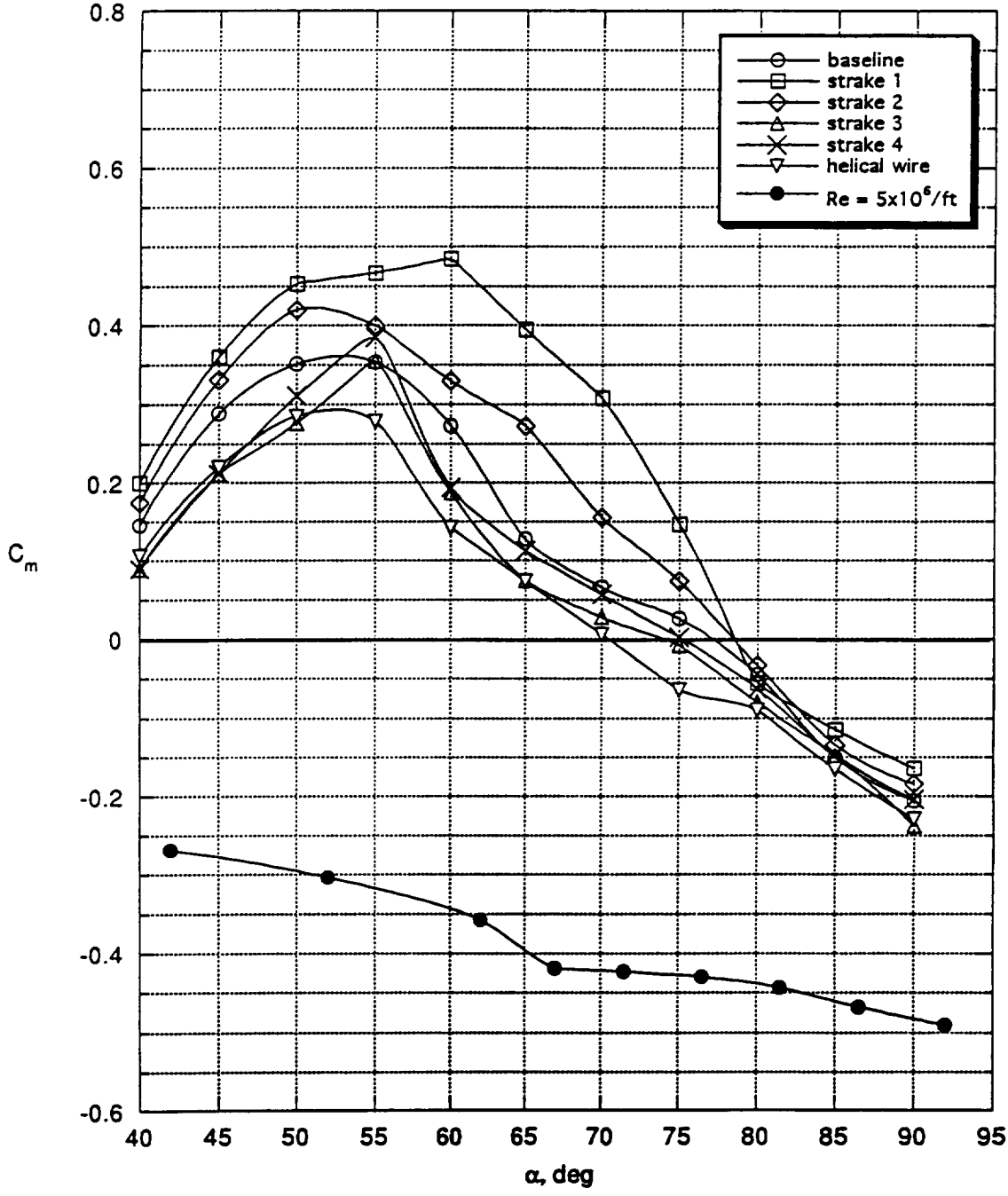

(a) $\beta = -10°$.

Figure 11. Static pitching moment characteristics of the X-29A at low- and high-Reynolds numbers, including the effects of forebody modifications. Sideslip angle is constant.
(δ_c=-60°, δ_a=25°, δ_s=30°, δ_r=0°)

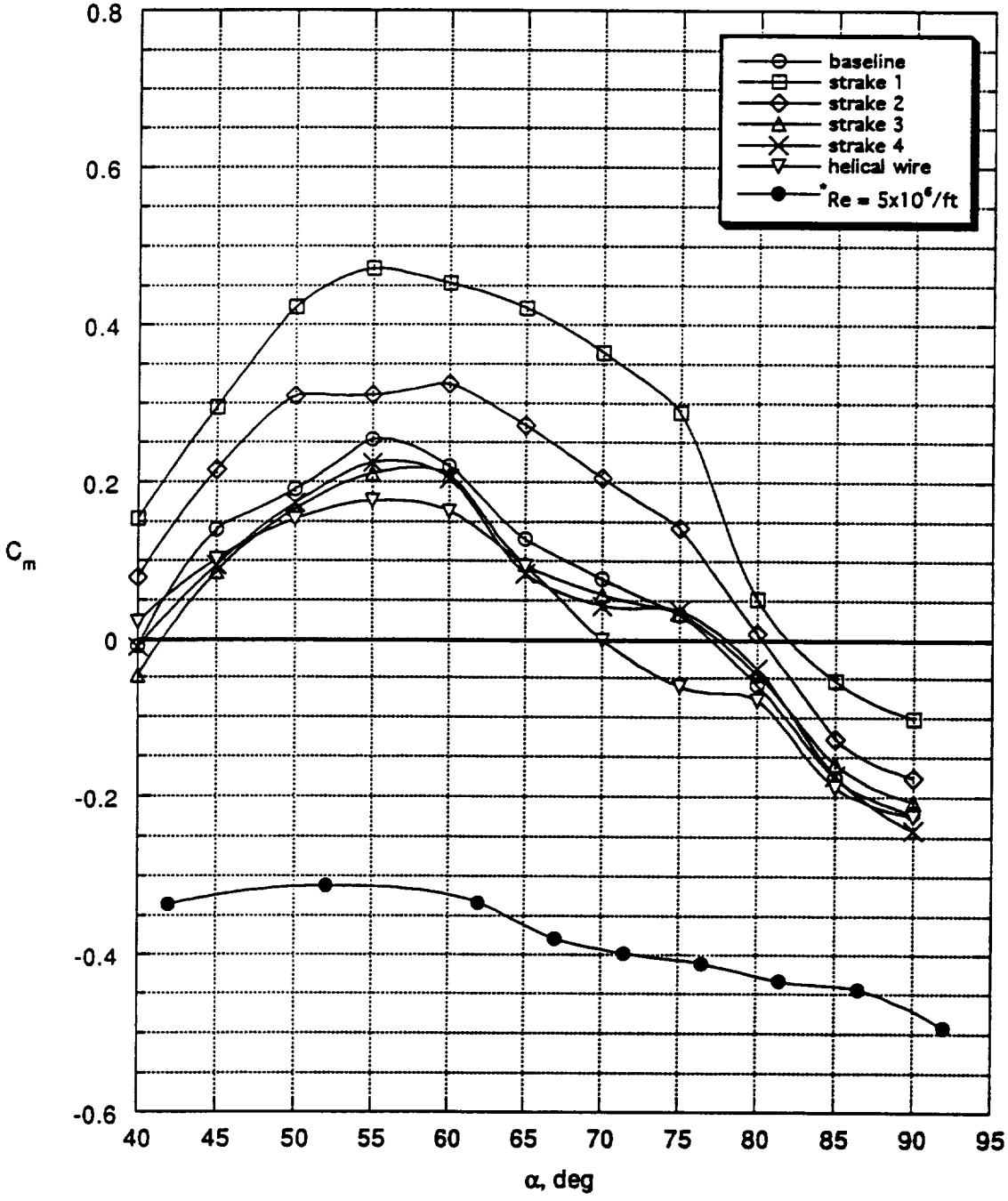

(b) $\beta = -5°$ ($^*\beta = -4°$ for Re=5x10^6/ft).

Figure 11. Continued.

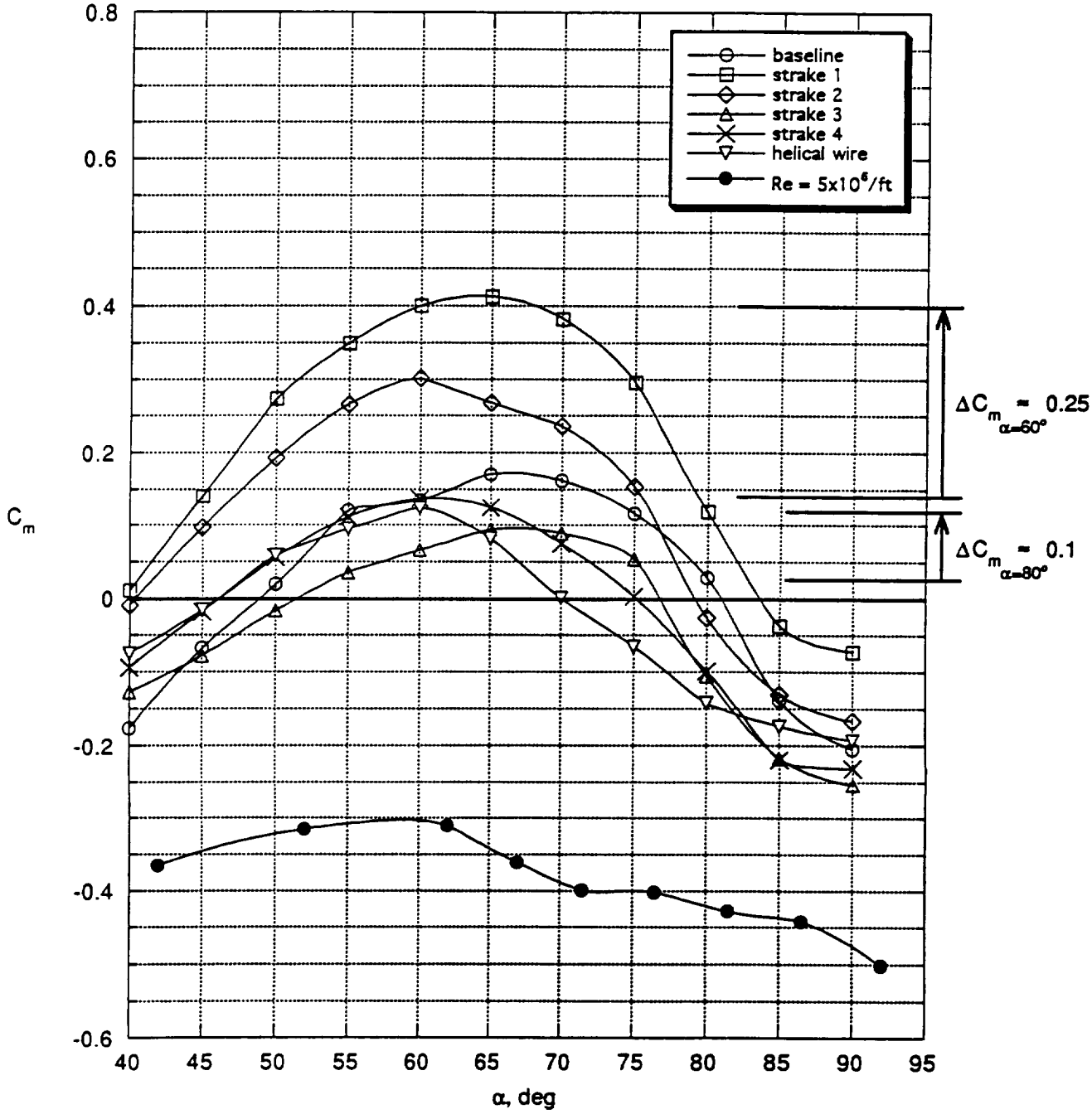

(c) $\beta = 0°$ (ΔC_m measured between baseline curve and strake 1 curve).

Figure 11. Continued.

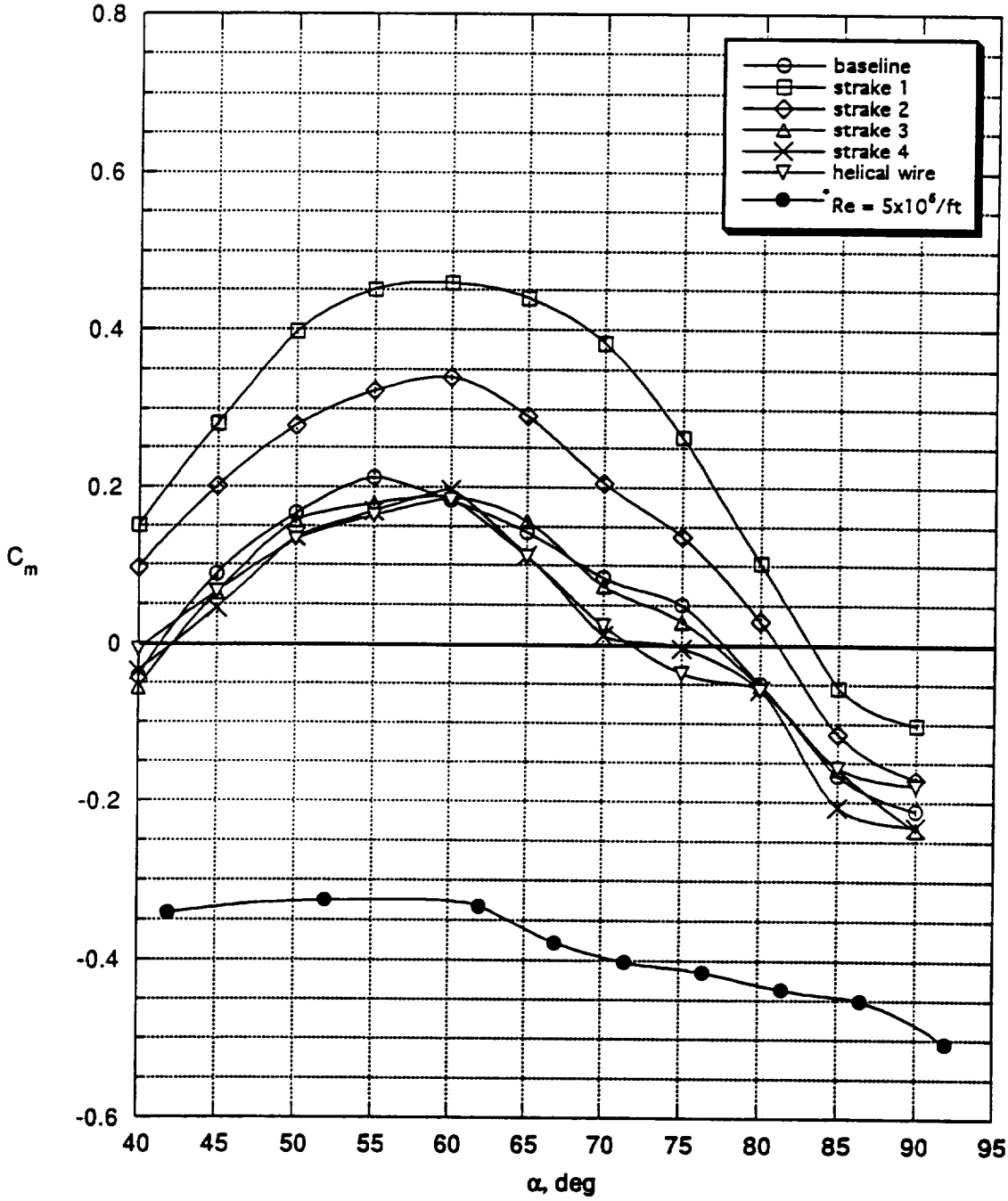

(d) $\beta = 5^\circ$ ($^*\beta = 4^\circ$ for Re=5x10^6/ft).

Figure 11. Continued.

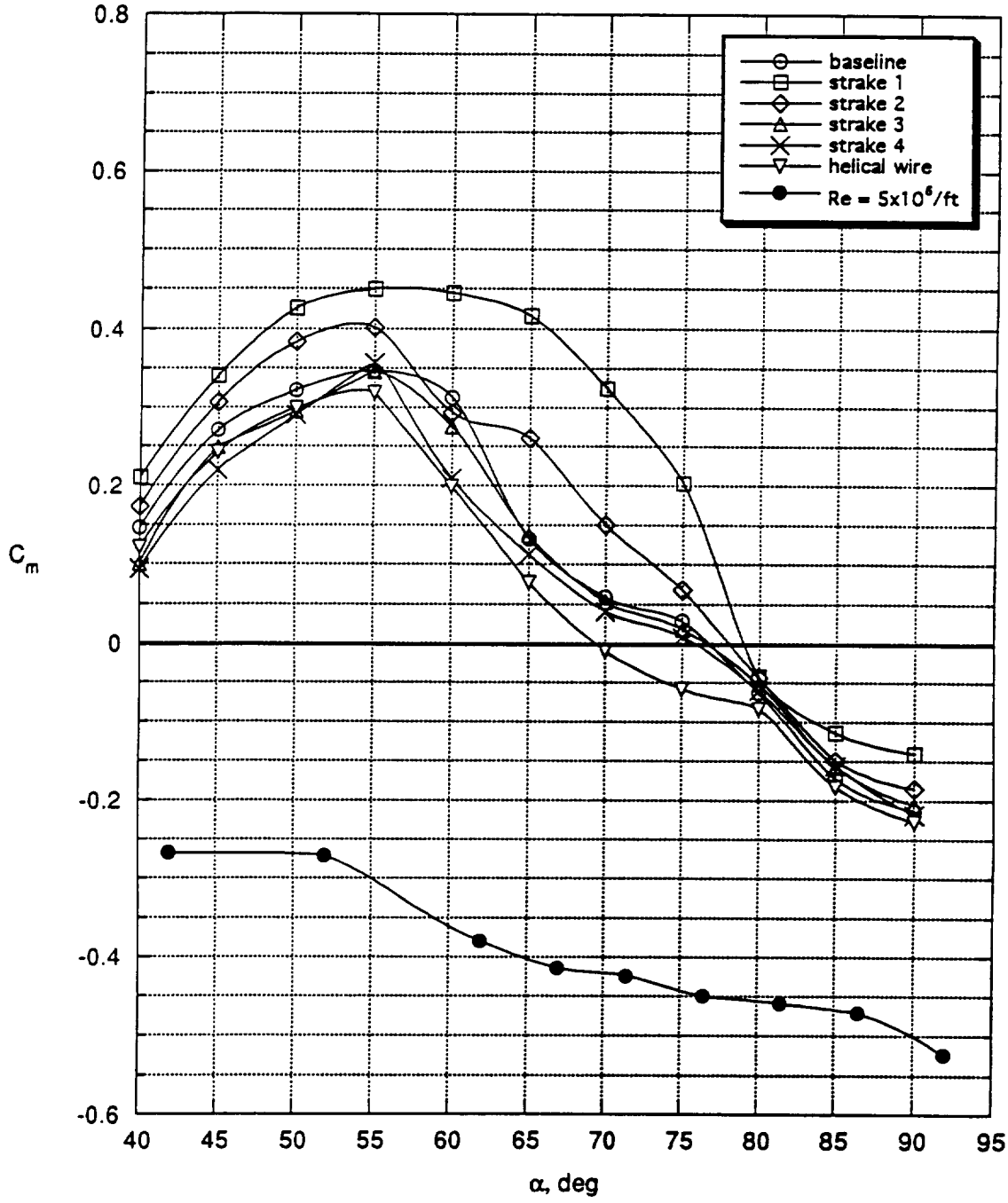

(e) $\beta = 10°$.

Figure 11. Continued.

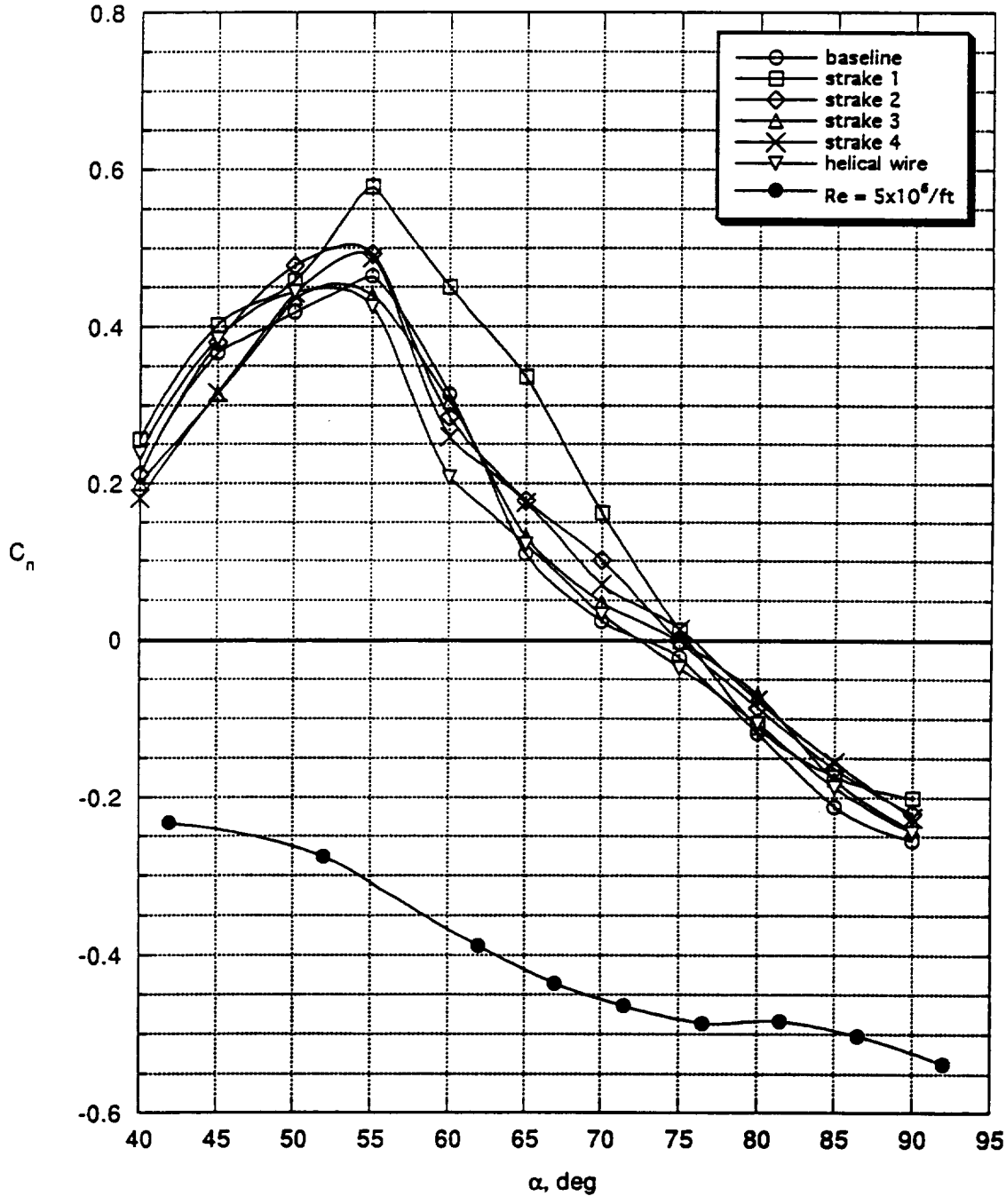

(f) $\beta = 15°$.

Figure 11. Continued.

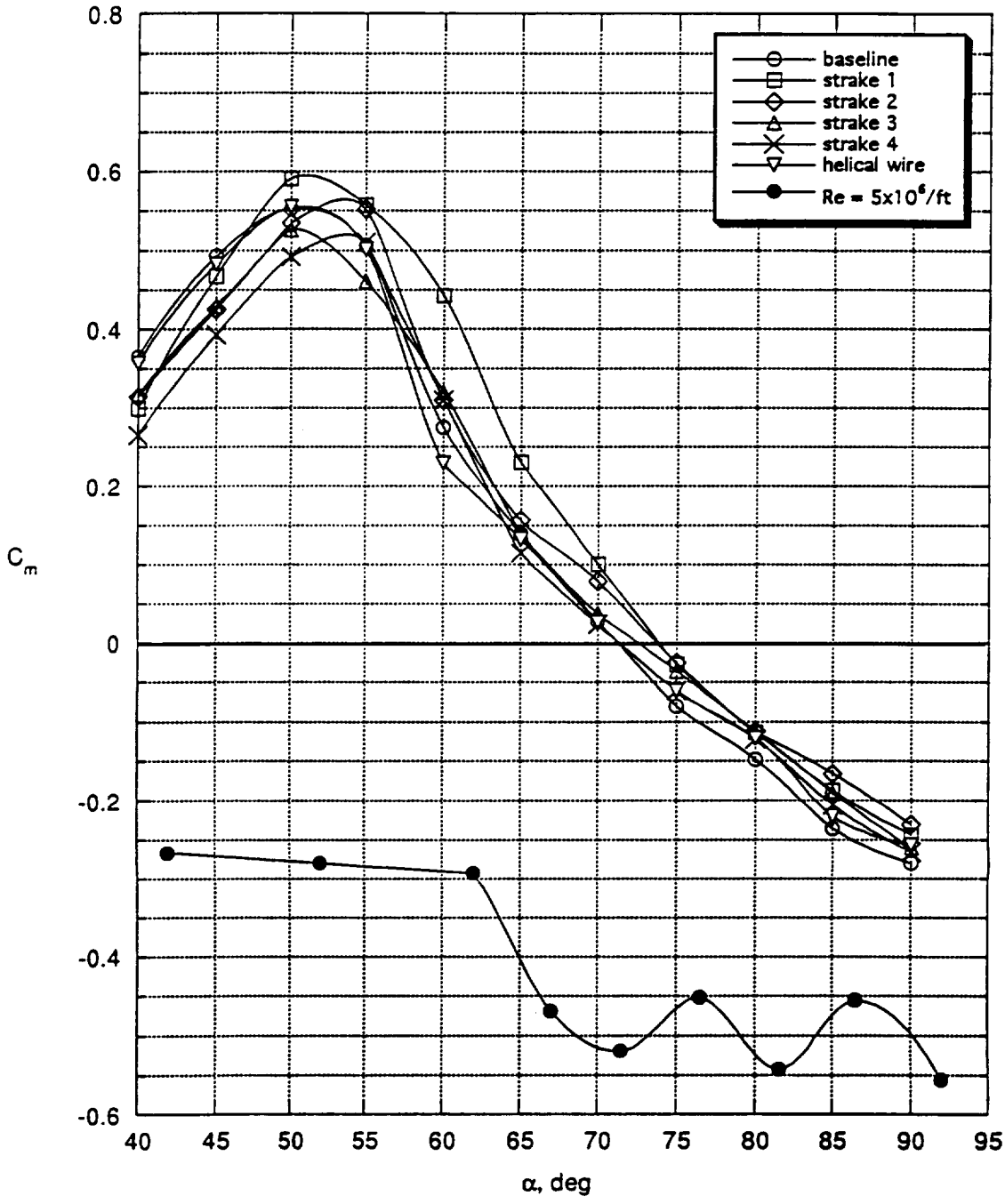

(g) $\beta = 20°$.

Figure 11. Continued.

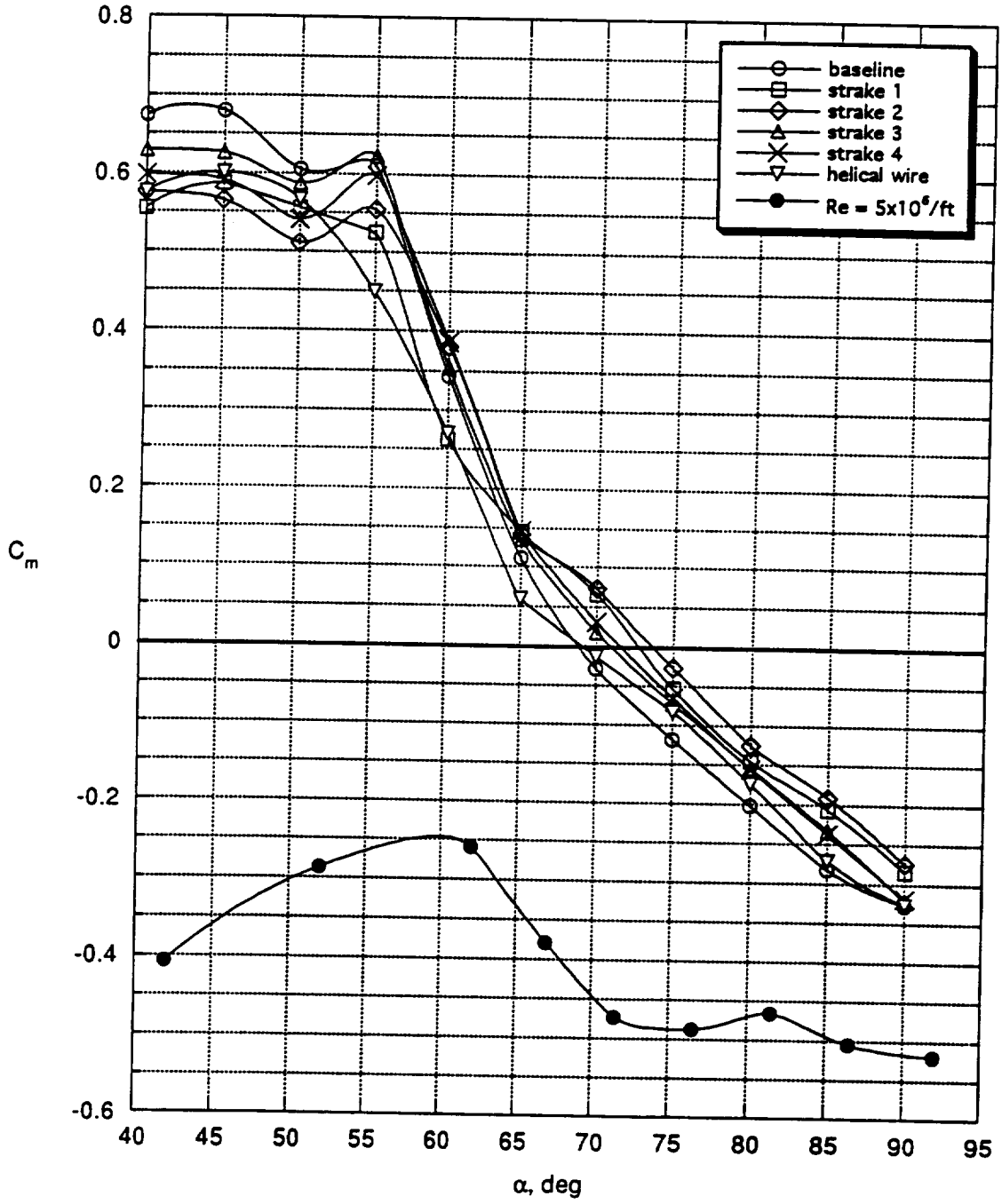

(h) β = 30°.

Figure 11. Concluded.

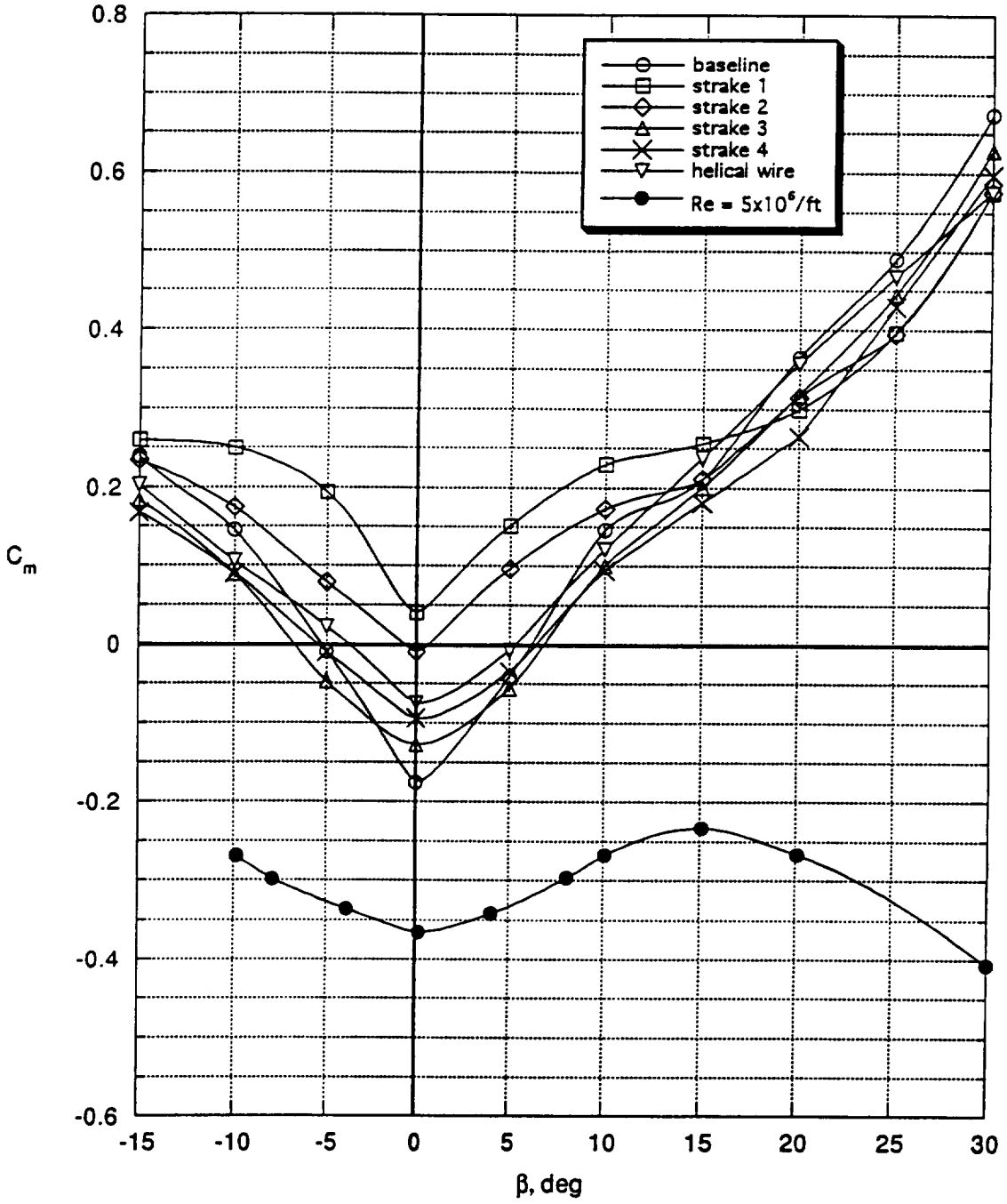

(a) $\alpha = 40°$.

Figure 12. Static pitching moment characteristics of the X-29A at low- and high-Reynolds numbers, including the effects of forebody modifications. Angle of attack is constant.

(δ_c=-60°, δ_a=25°, δ_s=30°, δ_r=0°)

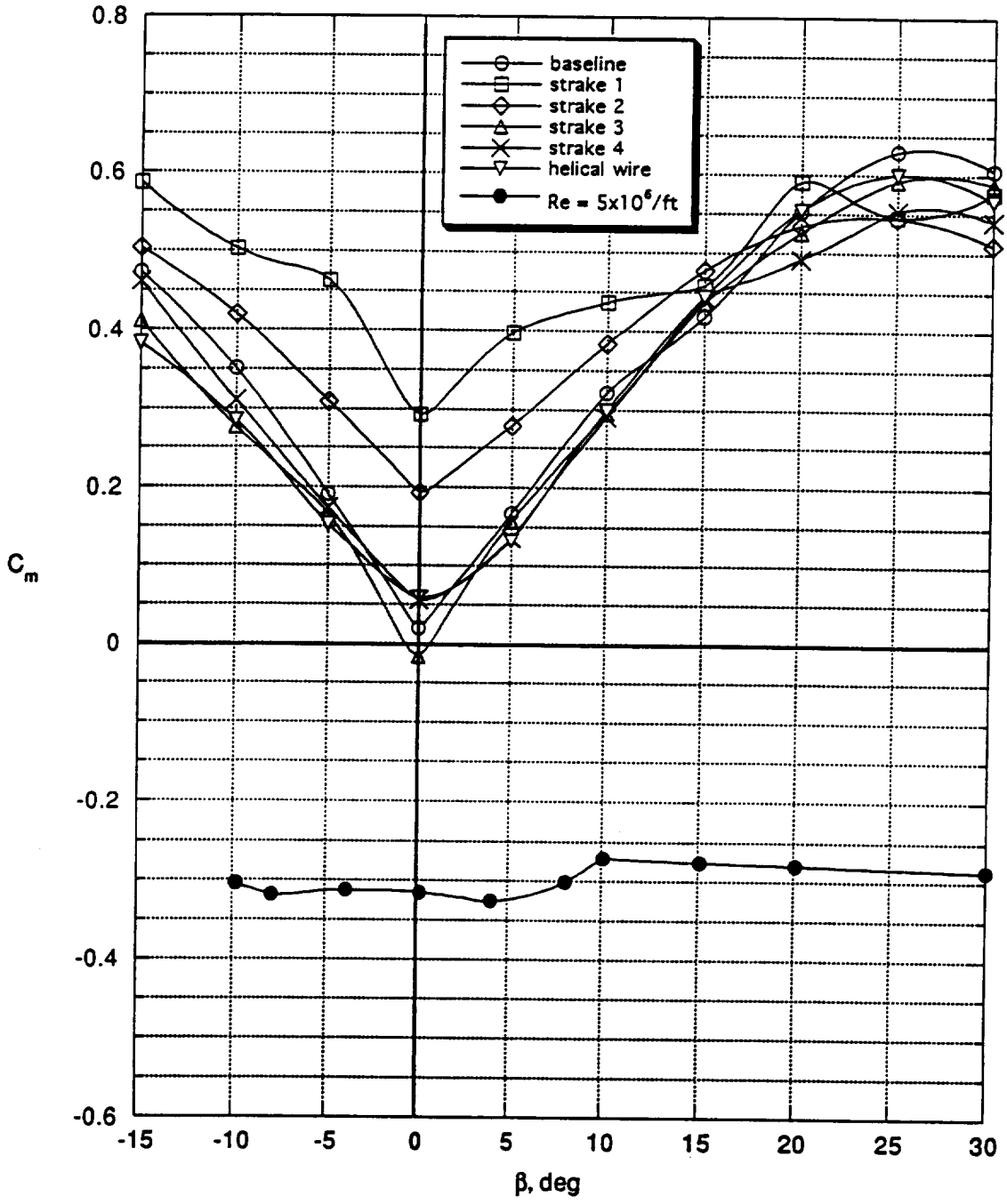

(b) $\alpha = 50°$.

Figure 12. Continued.

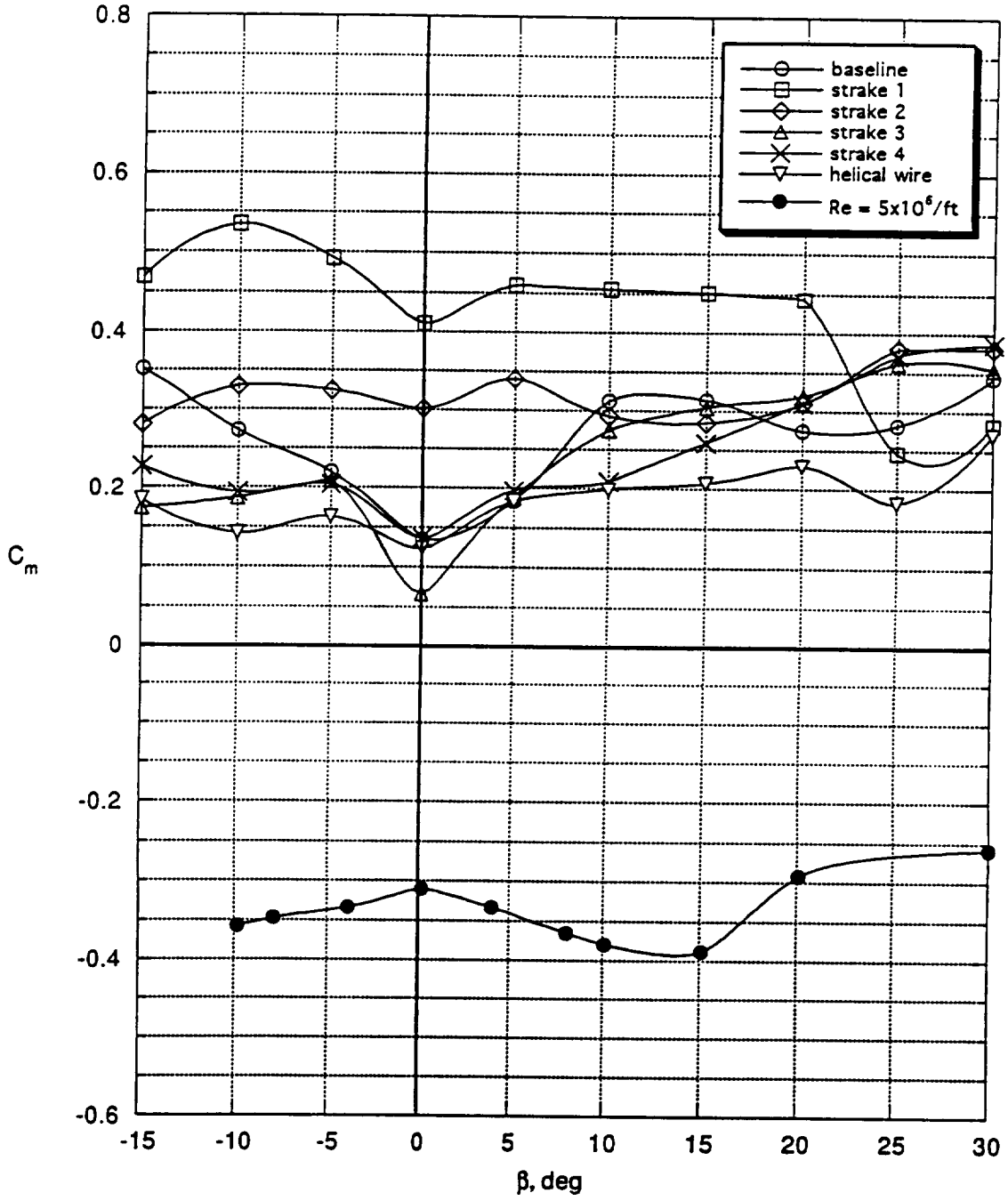

(c) $\alpha = 60°$.

Figure 12. Continued.

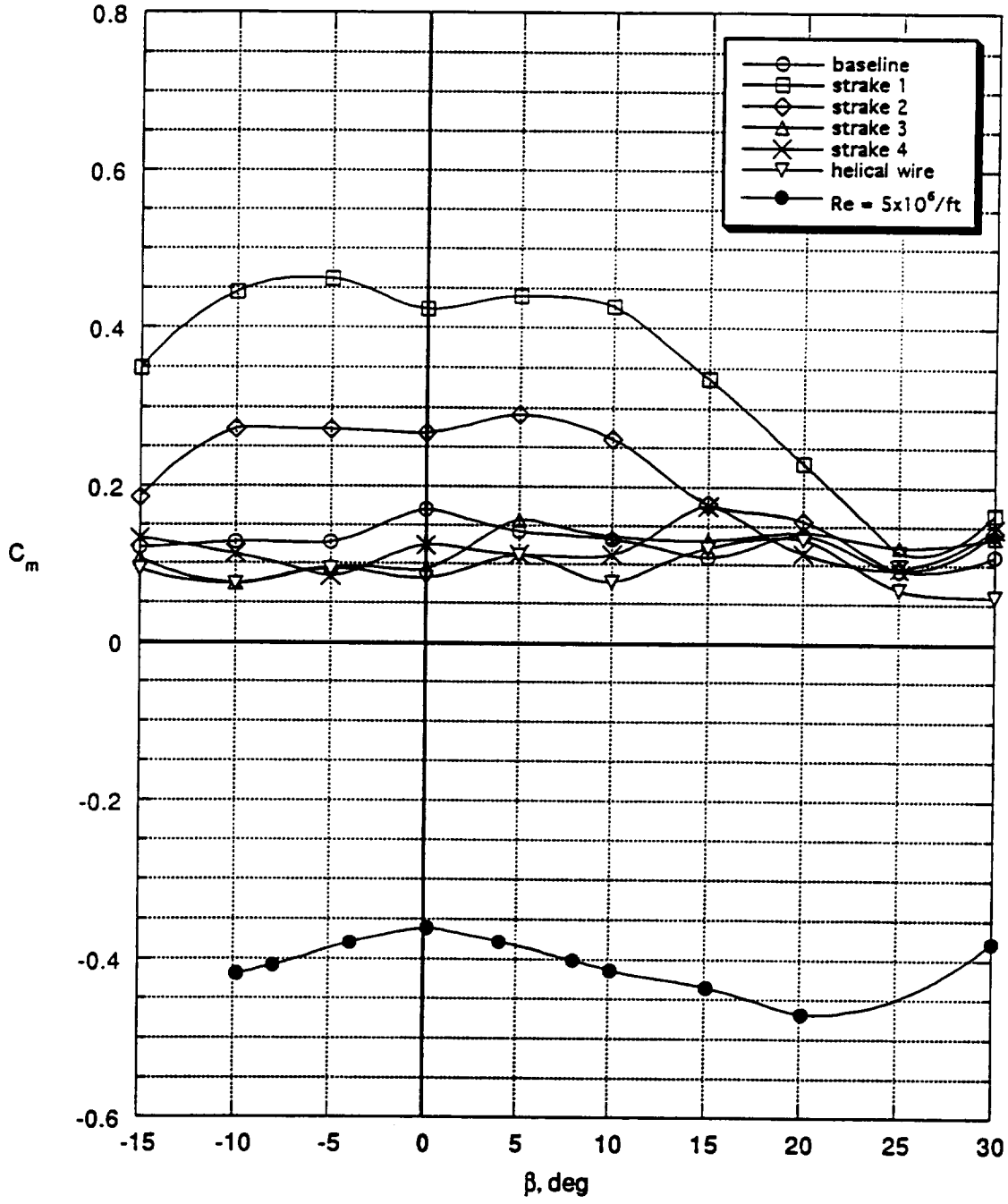

(d) $\alpha = 65°$.

Figure 12. Continued.

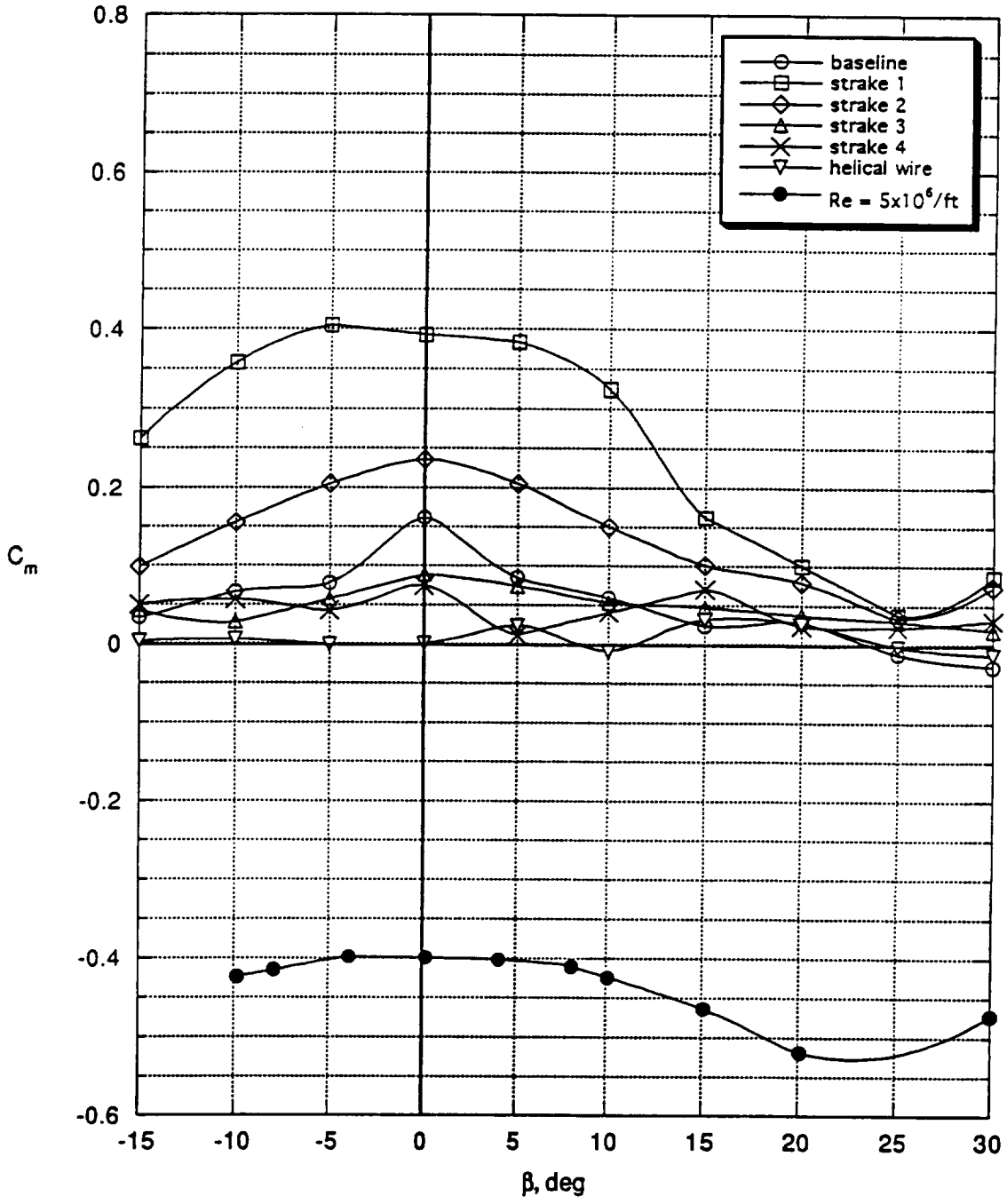

(e) $\alpha = 70°$.

Figure 12. Continued.

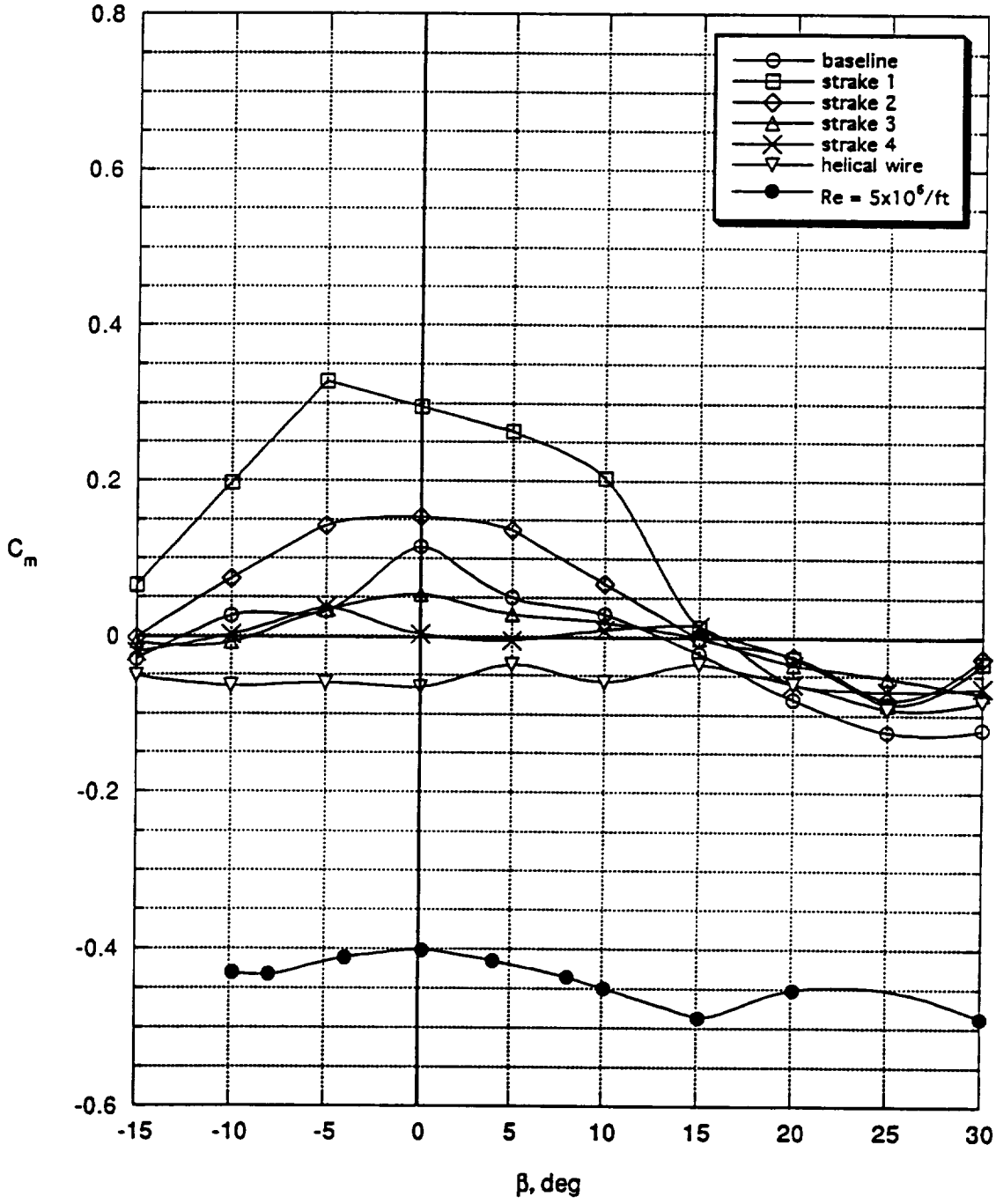

(f) $\alpha = 75°$.

Figure 12. Continued.

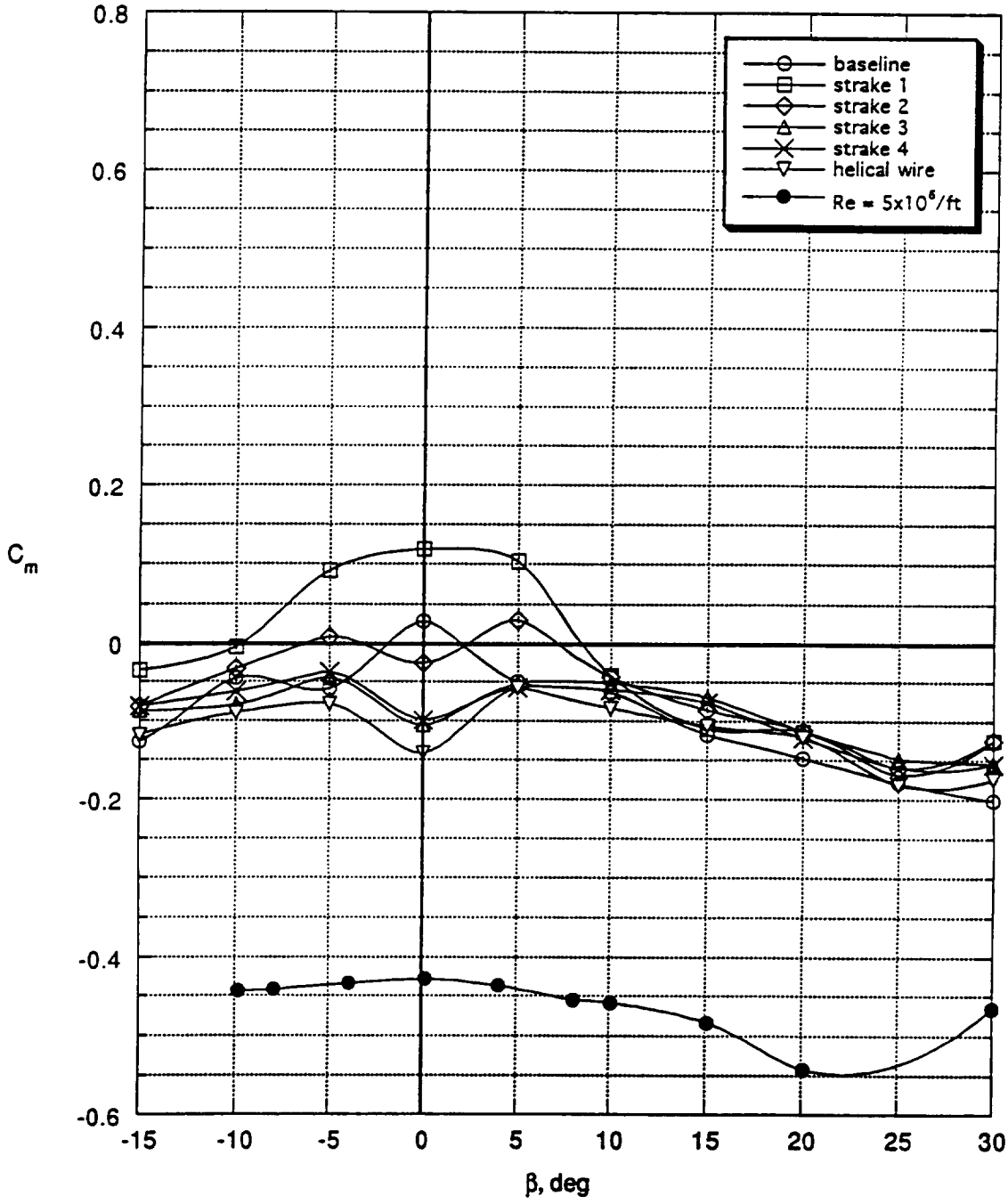

(g) $\alpha = 80°$.

Figure 12. Continued.

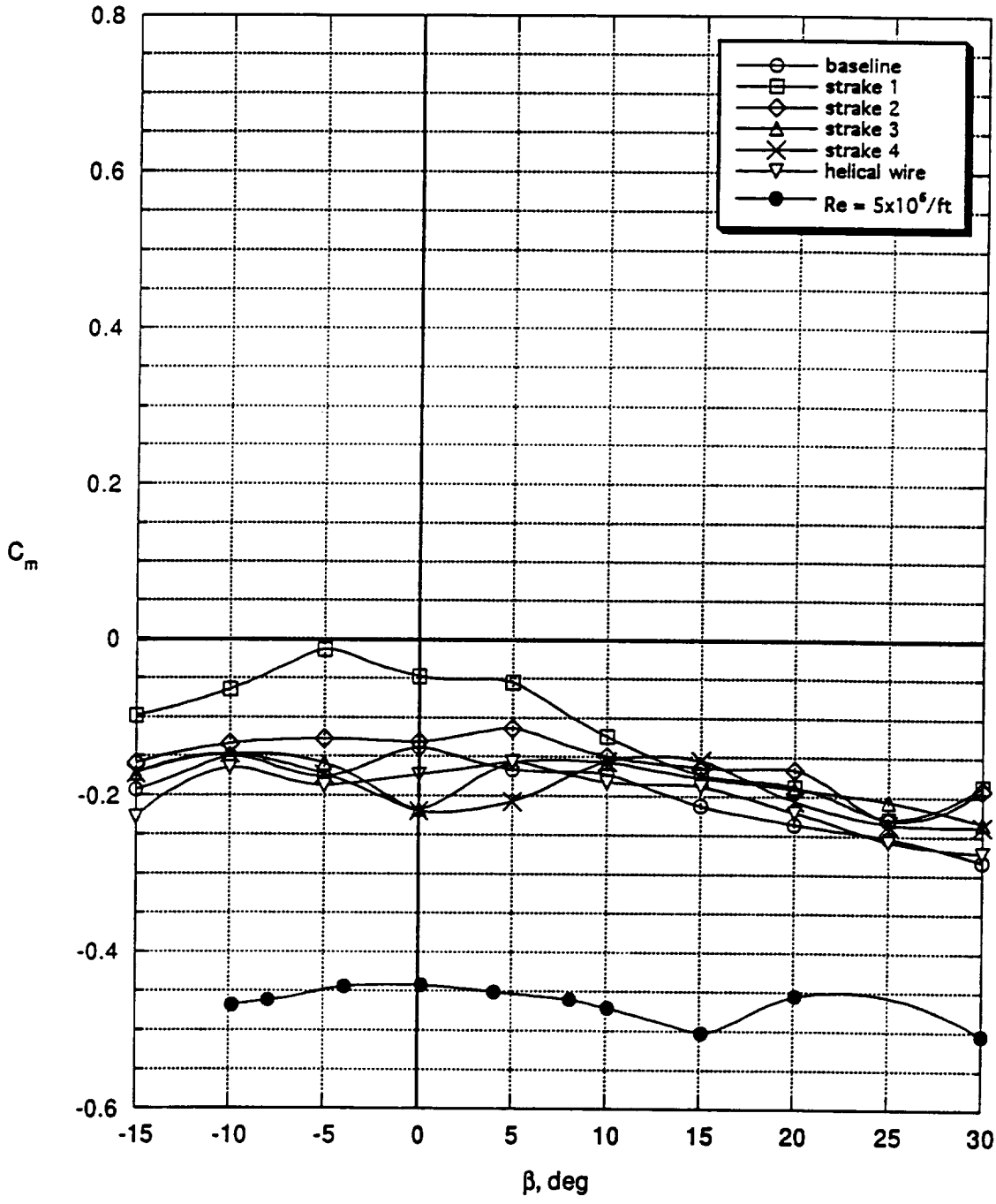

(h) $\alpha = 85°$.

Figure 12. Continued.

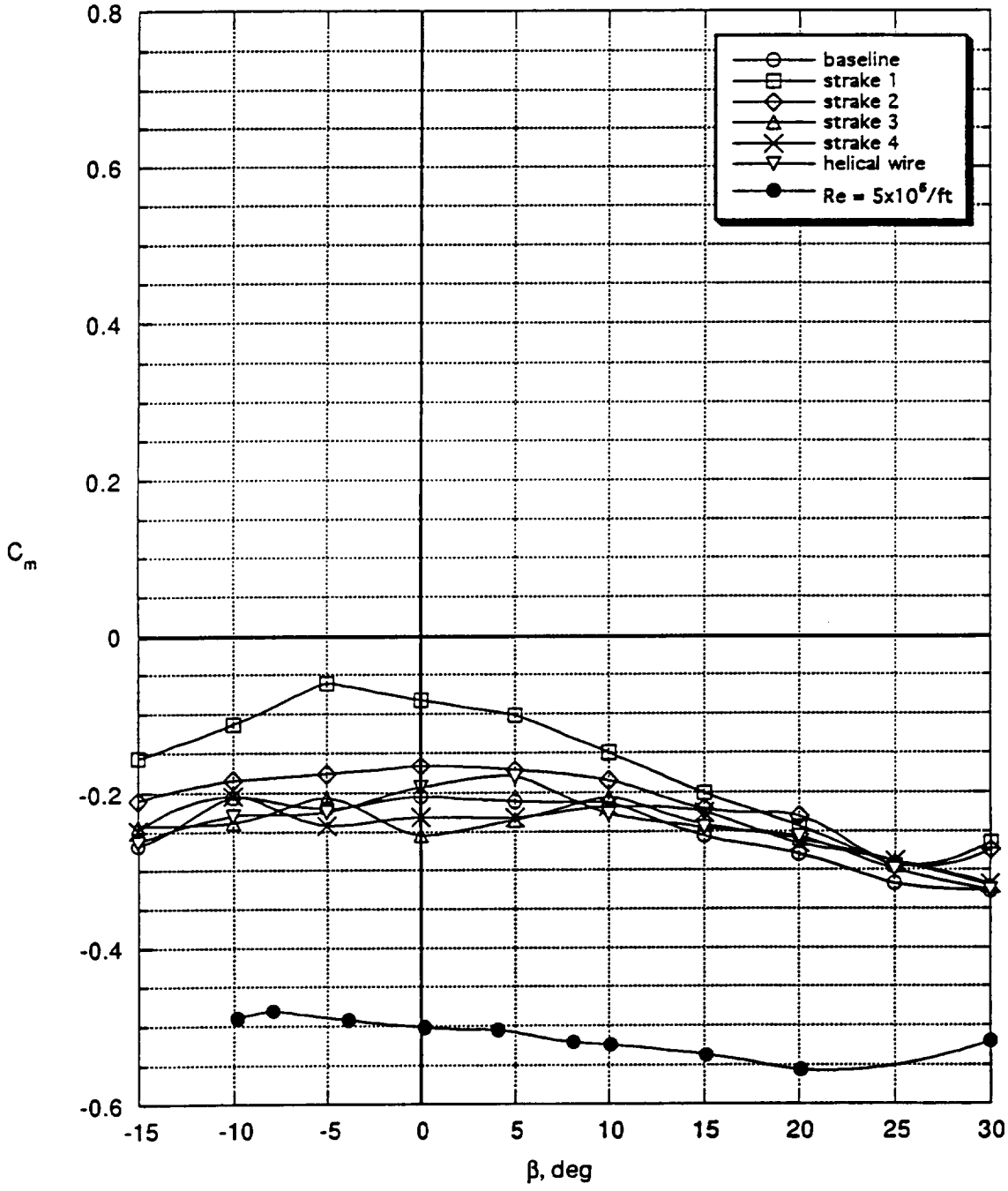

(i) $\alpha = 90°$.

Figure 12. Concluded.

REPORT DOCUMENTATION PAGE

Form Approved
OMB No. 0704-0188

1. AGENCY USE ONLY (Leave blank)	2. REPORT DATE	3. REPORT TYPE AND DATES COVERED
	March 1996	Contractor Report

4. TITLE AND SUBTITLE
Wind-Tunnel Parametric Investigation of Forebody Devices for Correcting Low Reynolds Number Aerodynamic Characteristics at Spinning Attitudes

5. FUNDING NUMBERS
C NAS1-19000
WU 505-68-70-05

6. AUTHOR(S)
C. Michael Fremaux

7. PERFORMING ORGANIZATION NAME(S) AND ADDRESS(ES)
Lockheed Engineering and Sciences Company
144 Research Drive
Hampton, VA 23666

8. PERFORMING ORGANIZATION REPORT NUMBER

9. SPONSORING / MONITORING AGENCY NAME(S) AND ADDRESS(ES)
National Aeronautics and Space Administration
Langley Research Center
Hampton, VA 23681-0001

10. SPONSORING / MONITORING AGENCY REPORT NUMBER
NASA CR-198321

11. SUPPLEMENTARY NOTES
Langley Technical Monitor: Raymond D. Whipple

12a. DISTRIBUTION / AVAILABILITY STATEMENT
Unclassified - Unlimited
Subject Category 08

12b. DISTRIBUTION CODE

13. ABSTRACT *(Maximum 200 words)*

An investigation has been conducted in the NASA Langley 20-Foot Vertical Spin Tunnel to determine the static aerodynamic characteristics of a 1/25-scale model of the X-29A Forward Swept Wing airplane. The tests were conducted at a free-stream dynamic pressure of 3.6 psf, corresponding to a unit Reynolds number of 0.35 million per foot, or 45,000 based on a maximum fuselage forebody depth of 0.128ft. The purpose of this investigation was to assess the ability of various forebody devices to correct the aerodynamic parameters that are important in spin testing for Reynolds number effects. Low Reynolds number aerodynamic characteristics obtained for the X-29A during the present test were compared with high Reynolds number data obtained for this configuration in a previous test. The low Reynolds number tests were conducted first with the unmodified (baseline) model and then repeated with each of several forebody modifications installed.

14. SUBJECT TERMS
Reynolds number, spinning, high angle of attack

15. NUMBER OF PAGES
56

16. PRICE CODE
A04

17. SECURITY CLASSIFICATION OF REPORT	18. SECURITY CLASSIFICATION OF THIS PAGE	19. SECURITY CLASSIFICATION OF ABSTRACT	20. LIMITATION OF ABSTRACT
Unclassified	Unclassified	Unclassified	